Abstract

ELECTROCHEMICAL DETECTION OF BENZO[*A*]PYRENE METABOLITE DNA DAMAGE: IMPLICATIONS OF NUCLEOBASE SEQUENCE AND ADDUCT STEREOCHEMISTRY

By
Jennifer Elizabeth Satterwhite
June, 2011

Director of Thesis: Dr. Eli Hvastkovs

Major Department: Chemistry

Xenobiotics are chemical compounds introduced to living organisms that originate outside the body. A well-studied xenobiotic is benzo[*a*]pyrene (BP), a polyaromatic hydrocarbon (PAH) primarily introduced into the body via cigarette smoke as well as through environmental pollution. Once inside the body, BP is ultimately metabolized into electrophilic benzo[*a*]pyrene- 7,8-diol-9,10-epoxide (BPDE) that reacts with and damages nucleophilic biomaterial, including DNA. BPDE predominately targets specific genomic guanines at sites termed hotspots. BPDE hotspot damage can result in DNA mutations that alter key amino acids in proteins that are involved in cellular regulation, eventually leading to cancer. This process occurs regularly in vivo within the *TP53* gene at selected codons. *TP53* codes for the p53 protein, which is involved in cellular apoptosis. BPDE stereochemistry and cytosine methylation within hotspot codons are also important parameters that affect the eventual mutagenesis stemming from BPDE-guanine adducts.

Traditional detection of site-specific DNA damage can be expensive and time consuming. Electrochemical approaches can remedy these drawbacks. An electrochemical sensor was developed to detect DNA damage from (±)-*anti*-BPDE. A double stranded DNA (dsDNA) oligomer corresponding to a known hotspot sequence in the *TP53* gene was immobilized on a

gold electrode and then exposed to BPDE. Voltammetric measurements were then performed in the presence of electroactive $C_{12}H_{25}V^{2+}C_6H_{12}V^{2+}C_{12}H_{25}$ (V^{2+} =4,4'-bipyridyl or viologen, C_{12}Viologen). BPDE exposure causes DNA structural changes through the formation of bulky adducts that influence the C_{12}Viologen-DNA interaction. These structural changes affect the resulting C_{12}Viologen voltammetry. At wild type *TP53* sequences, BPDE exposure resulted in the emergence of a positive shifted C_{12}Viologen redox wave at -0.37 V. At an identical sequence containing 5-methylated cytosine at the hotspot location, two waves emerged at -0.37 V and -0.54 V. These redox signals were muted when DNA was exposed to alternate xenobiotics or alternate sequences were exposed to BPDE. Overall, this demonstrates sequence specific detection of DNA damage at this hotspot sequence. Differences in the voltammetric response suggest that the sensor is sensitive to the adduct stereochemistry.

Additional studies were performed to monitor the effects of BP activation. Activation includes chemical oxidation of BP through association with reactive oxygen species or metabolism. Initial studies focused on the reaction of BP with DNA in the presence of hydrogen peroxide. DNA exposed to this reaction cocktail provided C_{12}Viologen voltammetry that was similar to that caused by BPDE exposure, highlighted by a large SWV current increase at -0.37 V. Results were consistent with Fenton chemistry occurring in the damage buffer producing hydroxyl radicals from hydrogen peroxide and iron impurities. The hydroxyl radicals appear to activate BP producing a reactive species that results in BP-DNA adducts.

Overall, the data show a sequence-specific DNA hybridized sensor has the capability of providing hotspot and stereospecific genotoxicity information for benzo[*a*]pyrene derivatives.

ELECTROCHEMICAL DETECTION OF BENZO[*A*]PYRENE METABOLITE DNA DAMAGE: IMPLICATIONS OF NUCLEOBASE SEQUENCE AND ADDUCT STEREOCHEMISTRY

By

Jennifer Elizabeth Satterwhite

A Thesis
Presented to the Faculty of the Department of Chemistry
East Carolina University
In Partial Fulfillment of the Requirements for the Degree
Masters of Science in Chemistry

East Carolina University, North Carolina
June, 2011

ELECTROCHEMICAL DETECTION OF BENZO[*A*]PYRENE METABOLITE DNA DAMAGE: IMPLICATIONS OF NUCLEOBASE SEQUENCE AND ADDUCT STEREOCHEMISTRY

by

Jennifer Elizabeth Satterwhite

APPROVED BY:

DIRECTOR OF
DISSERTATION/THESIS: _____
Eli G. Hvastkovs, PhD

COMMITTEE MEMBER: _____
Colin S. Burns, PhD

COMMITTEE MEMBER: _____
Allison S. Danell, PhD

COMMITTEE MEMBER: _____
Mary Farwell, PhD

COMMITTEE MEMBER: _____
Yu Yang, PhD

CHAIR OF THE DEPARTMENT OF CHEMISTRY
_____
Rickey P. Hicks, PhD

DEAN OF THE GRADUATE
SCHOOL: _____
Paul J. Gemperline, PhD

ACKNOWLEDGEMENTS

I would like to thank my research advisor, Dr. Eli Hvastkovs, as well as my thesis committee Dr. Colin Burns, Dr. Allison Danell, Dr. Mary Farwell, and Dr. Yu Yang for their support, valuable guidance, help and patience throughout my Masters study.

I would like to gratefully acknowledge my family, James Warden and close friends for their personal sacrifices, support, encouragement, and patience that enabled me to complete this work.

TABLE OF CONTENTS

LIST OF TABLES

LIST OF FIGURES

LIST OF SYMBOLS AND ABBREVIATIONS

AQMS	Anthraquinone-2-sulfonic acid
A/V	Amperes per Volts
Γ_o	Amount of redox molecule at electrode surface (mol cm^{-2})
N_A	Avogadro's number
BP	Benzo[*a*]pyrene
BPDE	Benzo[a]pyrene-7,8-dihydrodiol-9,10-epoxide
C_o^*	Bulk solution concentration (mol cm^{-3})
BHA	Butylated hydroxyanisole
Q_{dl}	Capacitive charge (μC, C)
cm^2	Centimeters squared
$^\circ C$	Celsius
ΔT_m	Change in melting transition
Q	Charge (μC, C)
z	Charge of redox molecule
CC	Chronocoulometry
con	Control
C	Coulombs
C_{12}Viologen	$C_{12}H_{25}V^{2+}C_6H_{12}V^{2+}C_{12}H_{25}$ (V^{2+} =4,4'-bipyridyl or viologen)
CV	Cyclic voltammetry
cyt P450	Cytochrome P450
DNA	Deoxyribonucleic acid
D_o	Diffusion coefficient (cm s^{-1})

Γ_{DNA}	DNA probe surface density
dsDNA	Double-stranded DNA
E-Buffer	Electrochemical buffer
ECL	Electrochemiluminescence
A	Electrode area (cm^2)
ESI	Electrospray ionization
EDTA	Ethylenediaminetetraacetic acid
F	Faraday's constant (9.65×10^4 C per mol e^-)
g	Grams
Au	Gold
Hz	Hertz (s^{-1})
HCS	High-content screening
hr	Hour
H_2O_2	Hydrogen peroxide
•OH	Hydroxyl radical
LMPCR	Ligation-mediated polymerase chain reaction
m/z	Mass-to-charge ratio
MS	Mass spectrometry
MHz	Megahertz
T_m	Melting transition
MCH	Mercaptohexanol
5-mC	5-methylcytosine
me	Methylated

$\mu C/cm^2$	Microcoulomb per centimeters squared
μL	Microliter
μm	Micrometer
μM	Micromolar
Mg	Milligrams
mL	Milliliter
mm	Millimeter
mM	Millimolar
$mV\ s^{-1}$	Millivolts per second
min	Minute
M	Molar
$mol\ cm^{-2}$	Moles per centimeter squared
Mb	Myoglobin
nM	Nanomolar
n	Number of electrons for reduction
PAH	Polyaromatic hydrocarbon
^1H NMR	Proton nuclear magnetic resonance
$V^{\bullet+}$	Reduced cation radical viologen
RuHex	Ruthenium hexamine
s	Seconds
ss1	Single strand 1
ss2	Single strand 2
ssDNA	Single-stranded DNA

SWV	Square wave voltammetry
SO	Styrene oxide
THF	Tetrahydrofuran
TE Buffer	Tris-EDTA buffer
UV-Vis	Ultraviolet-Visible
V	Voltage
wt	Wild type

CHAPTER 1: INTRODUCTION

DNA Damage from Xenobiotics

The maintenance of genome integrity and fidelity is essential for the proper function and survival of an organism.[1, 2] Numerous endogenous and exogenous sources can cause DNA damage.[1, 2] Commonly studied genotoxic agents are xenobiotics, which are chemical compounds (drug or pollutant) introduced to living organisms that are not produced endogenously in the body. Living organisms are typically exposed to xenobiotics by ingestion of water, drugs, or food and by inhalation of car exhaust or cigarette smoke, to name a few.[3] Prolonged exposure to xenobiotics can eventually cause serious health problems.[4]

Bioactivation

Once a xenobiotic is ingested, the body begins processes to eliminate the compound. The more hydrophobic a xenobiotic, the more difficult it is to excrete from the body.[3] The human body utilizes metabolic processes to remove exogenous compounds, but metabolism does not always result in detoxification. Many xenobiotics are converted to reactive molecules through enzymatic processes.[1-4] This is called bioactivation.[1-4]

Genotoxicity

Bioactivated species can interact and damage biomaterial such as proteins and DNA, which is termed genotoxicity.[1] Genotoxicity can lead to permanent DNA mutations if the lesions are not effectively or correctly repaired.[1, 4] **Figure 1.1** illustrates the bioactivation and resultant genotoxicity of benzo[*a*]pyrene (BP), a well-studied polyaromatic hydrocarbon that can be introduced to the body through various avenues, mainly smoking.[5, 6]

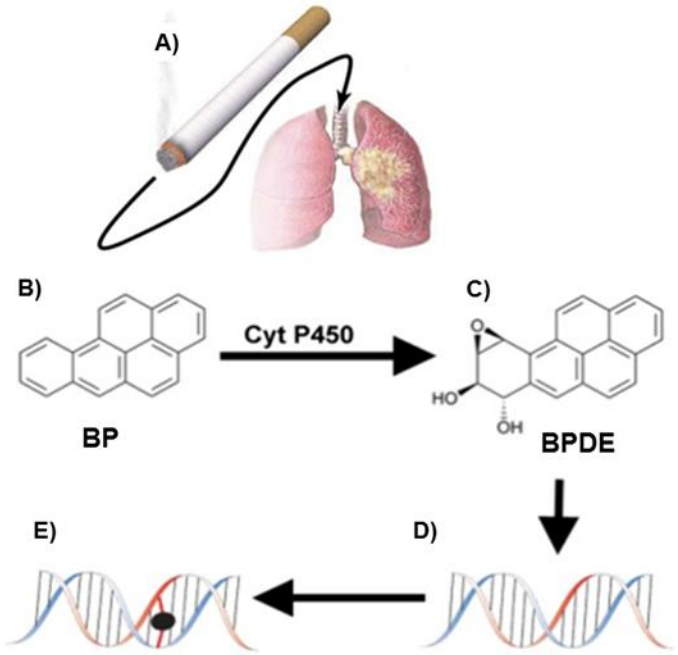

Figure 1.1: BP bioactivation to BPDE in the lung and DNA adduct formation.

The model provides an illustration of a BP molecule originating outside the body and upon metabolism carried out by mainly cytochrome P450 oxidases (cyt P450), it becomes a reactive, bioactivated metabolite benzo[*a*]pyrene-7,8-diol-9,10-epoxide (BPDE, **Figure 1.1c**).[4, 7] BPDE, the carcinogenic genotoxic metabolite, is electrophilic in nature and can react with nucleophilic DNA bases resulting in BPDE adducted DNA (**Figure 1.1e**).

Site-specific Genotoxicity

DNA damage from bioactivated xenobiotics does not necessarily occur at random nucleobases. Depending on the xenobiotic, DNA adducts occur at specific sites within the genome, termed "hotspots".[4, 8] BPDE has been shown to damage DNA at hotspot locations within the TP53 gene.[5] TP53 en codes the p53 protein, which is expressed as a cellular response to DNA damage in order to eventually promote apoptosis.[3, 9, 10] Studies have shown that DNA exposed to BPDE resulted in DNA damage at certain guanines in the TP53 gene, primarily codons 157, 248, and 273.[5] Mutations at these codons result in mutant p53 protein, and are frequently seen in lung cancer cells. **Figure 1.2** illustrates the mutation consequences resulting from site-specific BPDE-DNA damage at TP53 codon 273. If damage at the hotspot is not correctly repaired, the p53 transcription product will be changed by insertion of different amino

acids.[11] DNA mutations at the aforementioned hotspots affect amino acids involved in p53-DNA binding, altering the binding kinetics of the complex.[8, 11, 12] This is a key step in the formation of cancer.

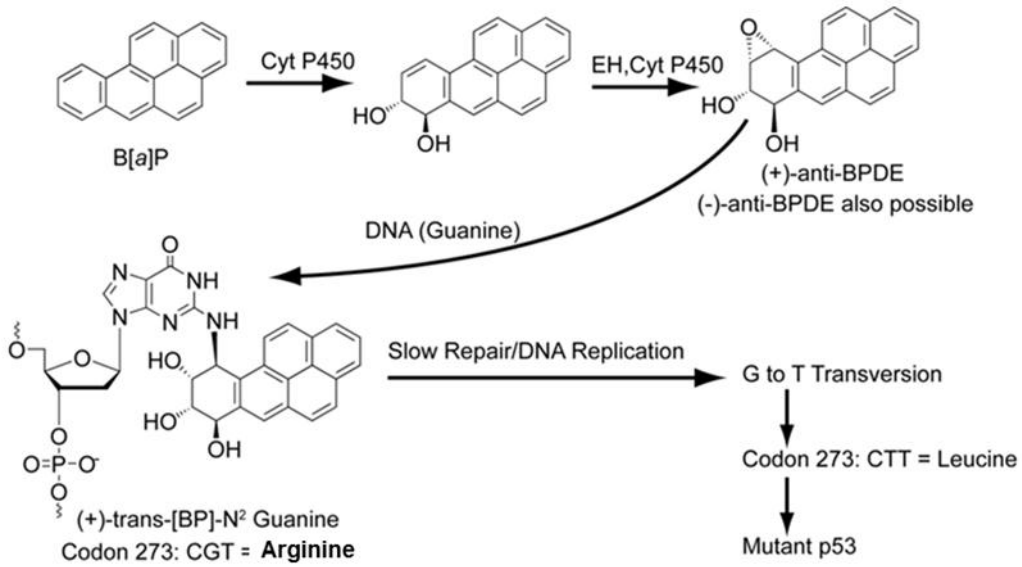

Figure 1.2: Illustration and genetic consequence of site specific DNA damage from BPDE at known TP53 gene codon 273 hotspot.

DNA Damage Influenced by Epigenetic Modifications

An epigenetic change is a modification to DNA that changes its function but does not affect the DNA sequence. An example is DNA methylation. DNA methylation typically occurs at CpG sites, sites where a cytosine nucleotide occurs beside a guanine in a DNA sequence.[13-15] Cytosine can be methylated at the 5-carbon location, as shown in **Figure 1.3**, termed 5-methylcytosine (5-mC).[14, 15] In human DNA, 60%-90% of the CpG sites contain 5-methylcytosine.[15] Methylation of the cytosine base plays an important role in genotoxicity. Studies

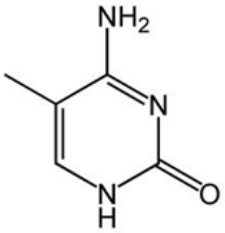

Figure 1.3: 5-methylcytosine is formed when the cytosine is methylated at the 5-carbon

have shown bulky xenobiotics, like BPDE, form DNA adducts preferentially at 5-mC sites.[5, 12-14] It has also been shown that the BPDE-DNA reaction is enhanced in the presence of 5-mC containing DNA sequences.

Detection Methods

DNA Hotspot Detection

Sequence-specific genotoxicity detection is not trivial. Studies have been performed to map the distribution of BPDE adducts within the p53 gene. Specifically, DNA was isolated from cells exposed to BPDE.[5, 12, 16, 17] DNA was treated with UvrABC nuclease, which specifically cleaves the damaged DNA at BPDE adduct sites.[5, 12, 16] Ligation-mediated polymerase chain reaction (LMPCR) was used to amplify the DNA fragments, followed by electrophoretic separation techniques.[5, 12, 16, 17] This method showed that BPDE preferentially adducts DNA primarily at guanines at codons 248, 249, and 273.[5]

One drawback to this technique is that it did not account for metabolism (bioactivation) of BP, even though this process plays a vital role in genotoxicity. The assay provided information regarding the actual damage site, but it is expensive, time-consuming and the data analysis is tedious.

DNA Damage Detection

Several established assays have been utilized to detect for genotoxicity resulting from xenobiotic exposure. The most well-known is the Ames assay.[18, 19] This assay consists of exposing a xenobiotic to bacteria that are unable to grow in certain medium. Genotoxic exposure causes mutations in the bacteria that allow for the synthesis of an amino acid that allows the bacteria to grow.[18, 19] The bacteria grow in a dose dependent manner; therefore, the number of colonies that form is used to ascertain the genotoxic potential of many xenobiotics from

environmental carcinogens to pharmaceutical compound candidates.[18, 19] Metabolism processes can be incorporated into the Ames test, which can often introduce several problems.[19, 20] This technique provides an overall picture of the genotoxic potential for a xenobiotic, but does not provide detailed information, such as DNA sequence effects leading to preferentially adducted hotspots or other molecular level information.

Newer biosensor genotoxicity detection schemes have been developed to try and remedy some of the drawbacks of the classical genotoxicity assays. Biosensors are integrated analytical devices that couple a biorecognition interface with a transducer.[21, 22] There are several different biosensors that differ based on the bio element and transducing mechanism. The biosensor format is cost efficient, simpler and has the potential to be used for early toxicity screening. Several different optical and electrochemical biosensing approaches have been developed. High-content screening (HCS) enables the detection and evaluation of multiple biochemical and morphology parameters in cellular conditions by combining fluorescent signals and auto imaging.[19, 23] HCS was used to predict hepatotoxicity for 90% of a sample set of drugs that induced varying liver toxicity levels.[19, 23] An optical design using rat hepatocytes immobilized on porous silica was used to monitor biological events and real-time cellular viability by measuring increases in scattered light after exposure to xenobiotics.[19, 24] The intensity of the light increased demonstrating the changing cell structure due to xenobiotic exposure.[24] Electrochemical DNA damage detection biosensors have employed thin films containing alternating layers of DNA and enzymes.[19, 25] Enzymes within the films produced reactive metabolites that damaged DNA. DNA damage was detected using electrochemiluminescence from an imbedded redox polymer that interacted with damaged guanines in DNA.[25, 26] DNA adducts were also measured using LC-MS techniques.[19, 25] Similar approaches were used to monitor oxidative stress to assess drug toxicity.

Oxidative damage resulting in 8-oxoguanine formation was detected using a redox active polymer film that selectively detected this form of genotoxicity.[25]

Electrochemical Hybridization Sensor

An electrochemical DNA hybridization biosensor utilizes the DNA sequence of interest as the biorecognition interface while the transducer is an electrode on which the DNA is immobilized. Once the hybridized sensor is constructed, label or label-free methods are used to obtain an electrochemical signal to measure the desired biochemical process.[21, 22] This is discussed in more detail below.

Immobilization of DNA on Biosensor

Two main approaches exist to immobilize DNA on an electrode. The first is non-specific adsorption of DNA directly at the surface.[21, 22] These methods typically rely on guanine oxidation techniques to assay the presence of DNA at the electrode. The other immobilization approach is the specific adsorption of DNA through the formation of a self-assembled monolayer (SAM) on gold electrodes.[21] This technique is characterized by specific adsorption of DNA at the gold electrode through a thiol-linkage. First, a thiolated single-stranded DNA (ssDNA), called the probe, is immobilized on the surface. To then achieve high hybridization efficiency a reactive group, such as a mercaptohexanol, is used to passivate the unmodified electrode surface and lift non-specifically adsorbed ssDNA from the surface, positioning the probes to project out into solution.[21] Hybridized double stranded DNA (dsDNA) is formed after exposure to the complementary target strand.

Electrochemical Monitoring of DNA Hybridization

Label and label-free methods have been used to achieve an electrochemical signal that denotes the presence of dsDNA on an electrode. Label-free detection approaches rely on the

natural electroactivity of DNA.[21] Typically, guanine bases in DNA are oxidized at an electrode. Guanine oxidation occurs differently if the DNA is single-stranded compared to double-stranded, and this difference can be used to ascertain the DNA state. Labeled methods typically employ a redox active molecule that interacts selectively with DNA. [21, 22] For instance, studies showed that DNA π-stack perturbations could be detected using a terminally located redox-active intercalator.[27] Rhodium, based intercalators, binding in the DNA major groove have been used to detect DNA base mismatches.[28] Redox active dsDNA intercalator, anthraquinone-2-sulfonic acid (AQMS) was used to detect long-range charge transfer through dsDNA.[29, 30]

Electrochemical DNA hybridization detection is not limited to redox active intercalators. Molecules exploiting the structural changes related to dsDNA vs. ssDNA have also been used to detect hybridization at an electrode surface. dsDNA has a much more rigid structure than ssDNA, featuring minor and major grooves. Several minor groove binding molecules have been utilized to recognize dsDNA at an electrode surface. A diviologen derivative $C_{12}H_{25}V^{2+}C_6H_{12}V^{2+}C_{12}H_{25}$ (V^{2+} = 4,4′-bipyridyl or viologen, C_{12}Viologen) that interacts with the DNA minor groove has been used to ascertain DNA structural information.[31] C_{12}Viologen voltammetry was used to distinguish dsDNA from ssDNA. In the presence of dsDNA, C_{12}Viologen provided dual wave cyclic voltammetry, which was shown to be due to C_{12}Viologen dimer formation upon reduction in the presence of dsDNA.[31, 32]

Novel Electrochemical Approach

Remarkable progress has been made in the area of biosensors designed to detect genotoxicity, but still some challenges remain. Very few electrochemical biosensor approaches have been utilized to ascertain hotspot phenomena in the xenobiotic DNA damage process. Related to this, no existing biosensors truly tackle the molecular level information related to

DNA morphology or adduct stereochemistry, which are very important in determining the eventual toxicity of specific DNA adducts.

Genotoxicity testing is important in industry to provide DNA reactivity information for compounds of interest.[33] However, established genotoxicity screens and developing biosensor technologies are unable to provide pertinent information that answer disease-related questions, such as DNA damage site or adduct orientation.[11] Genotoxicity assays that provide molecular level information are expensive and time consuming.[34]

Electrochemical detection methods offer sensitivity coupled with benefits of low cost, high throughput and miniaturization. Therefore, an electrochemical detection platform that can rapidly analyze sequence-specific genotoxicity would be welcome. In this report, we present an electrochemical method to detect and study important genotoxic processes involving well-known carcinogens that damage DNA at specific genomic sites. A hybridized DNA sensor technique was employed to detect DNA damage from xenobiotics. Xenobiotic-induced DNA structural changes were monitored via responses from redox-active C_{12}Viologen. Chapter 3 describes the construction of electrochemical sensor using a known hotspot sequence from the TP53 gene. DNA was damaged with BPDE. C_{12}Viologen voltammetry was consistent with the formation of several different BPDE-DNA adducts, which can be explained through understanding BPDE adduct stereochemistry. In Chapter 4, we show the influence of epigenetic modifications (cytosine methylation) on the reactivity and binding of BPDE to DNA. The data suggest that BPDE binds differently in the presence of 5-methylcytosine producing adducts with altered stereochemical alignment. Finally, in Chapter 5, we studied BP activation through hydrogen peroxide. Our results suggest that the pro-carcinogen BP was activated by a hydroxyl radical to a reactive species producing DNA adducts. Overall, these results show the development of an

electrochemical sensor that has the ability to provide sequence-specific and stereospecific genotoxicity information for benzo[*a*]pyrene derivatives at selected TP53 hotspot oligomers.

References

(1) Schärer, O. D. Chemistry and Biology of DNA Repair. *Angewandte Chemie International Edition* **2003**, *42*, 2946-2974.

(2) Friedberg, E. C. DNA damage and repair. *Nature* **2003**, *421*, 436-440.

(3) Boelsterli, U. A. In *Mechanistic Toxicology: The Molecular Basis of How Chemicals Disrupt Biological Targets;* Taylor & Francis: London, **2003**, pp 1-3, 50-54, 207.

(4) Ortiz de Montellano, P. R. In *In Cytochrome P450: Structure, Mechanism, and Biochemistry;* Kluwer Academic/Plenu: New York, **2005.**

(5) Denissenko, M. F.; Pao, A.; Tang, M.; Pfeifer, G. P. Preferential Formation of Benzo[*a*]pyrene Adducts at Lung Cancer Mutational Hotspots in P53. *Science* **1996**, *274*, 430-432.

(6) Gelboin, H. V. Benzo[*a*]pyrene metabolism, activation and carcinogenesis: role and regulation of mixed-function oxidases and related enzymes. *Physiological Reviews* **1980**, *60*, 1107-1166.

(7) Kim, J. H.; Stansbury, K. H.; Walker, N. J.; Trush, M. A.; Strickland, P. T.; Sutter, T. R. Metabolism of benzo[*a*]pyrene and benzo[*a*]pyrene-7,8-diol by human cytochrome P450 1B1. *Carcinogenesis* **1998**, *19*, 1847-1853.

(8) Pfeifer, G.; Besaratinia, A. Mutational spectra of human cancer. *Human Genetics* **2009**, *125*, 493-506.

(9) Vogelstein, B.; Lane, D.; Levine, A. J. Surfing the p53 network. *Nature* **2000**, *408*, 307-310.

(10) Giono, L. E.; Manfredi, J. J. The p53 tumor suppressor participates in multiple cell cycle checkpoints. *J. Cell. Physiol.* **2006**, *209*, 13-20.

(11) Bullock, A. N.; Fersht, A. R. Rescuing the Function of Mutant p53. *Nature Reviews Cancer* **2001**, *1*, 68.

(12) Smith, L. E.; Denissenko, M. F.; Bennett, W. P.; Li, H.; Amin, S.; Tang, M.; Pfeifer, G. P. Targeting of Lung Cancer Mutational Hotspots by Polycyclic Aromatic Hydrocarbons. *Journal of the National Cancer Institute* **2000**, *92*, 803-811.

(13) Chen, J. X.; Zheng, Y.; West, M.; Tang, M. Carcinogens Preferentially Bind at Methylated CpG in the p53 Mutational Hot Spots. *Cancer Research* **1998**, *58*, 2070-2075.

(14) Denissenko, M. F.; Chen, J. X.; Tang, M.; Pfeifer, G. P. Cytosine methylation determines hot spots of DNA damage in the human P53 gene. *Proceedings of the National Academy of Sciences* **1997**, *94*, 3893-3898.

(15) Tornaletti, S.; Pfeifer, G. P. Complete and tissue-independent methylation of CpG sites in the p53 gene: implications for mutations in human cancers. *Oncogene* **1995**, *10*, 1493.

(16) Mikhail F Denissenko, Annie Pao, Gerd P Pfeifer and Moon-shong Tang. Slow repair of bulky DNA adducts along the nontranscribed strand of the human *p53* gene may explain the strand bias of transversion mutations in cancers. *Oncogene* **1998**, *16*, 1241.

(17) Feng, Z.; Hu, W.; Hu, Y.; Tang, M. Acrolein is a major cigarette-related lung cancer agent: Preferential binding at p53 mutational hotspots and inhibition of DNA repair *Proceedings of the National Academy of Sciences* **2006**, *103*, 15404-15409.

(18) Ames, B.; Mccann, J.; Yamasaki, E. Methods for detecting carcinogens and mutagens with the Salmonella/mammalian-microsome mutagenicity test. *Mutation Research* **1975**, *31*, 347-364.

(19) Rusling, J. F.; Hvastkovs, E. G.; Schenkman, J. B. In *Screening for Reactive Metabolites Using Genotoxicity Arrays and Enzyme/DNA Biocolloids;* Drug Metabolism Handbook; John Wiley & Sons, Inc.: **2009; 2008**; pp 307-340.

(20) Lutz, W. K. In vivo covalent binding of organic chemicals to DNA as a quantitative indicator in the process of chemical carcinogenesis. *Mutation Research/Reviews in Genetic Toxicology* **1979**, *65*, 289-356.

(21) Odenthal, K. J.; Gooding, J. J. An introduction to electrochemical DNA biosensors. *Analyst* **2007**, *132*, 603-610.

(22) Drummond, T. G.; Hill, M. G.; Barton, J. K. Electrochemical DNA sensors. *Natural Biotechnology* **2003**, *21*, 1192-1199.

(23) O'Brien, P.; Irwin, W.; Diaz, D.; Howard-Cofield, E.; Krejsa, C.; Slaughter, M.; Gao, B.; Kaludercic, N.; Angeline, A.; Bernardi, P.; Brain, P.; Hougham, C. High concordance of drug-induced human hepatotoxicity with in vitro cytotoxicity measured in a novel cell-based model using high content screening. *Archives of Toxicology* **2006**, *80*, 580-604.

(24) Schwartz, M. P.; Derfus, A. M.; Alvarez, S. D.; Bhatia, S. N.; Sailor, M. J. The Smart Petri Dish: A Nanostructured Photonic Crystal for Real-Time Monitoring of Living Cells. *Langmuir* **2006**, *22*, 7084-7090.

(25) Rusling, J. F.; Hvastkovs, E. G.; Schenkman, J. B. Toxicity screening using biosensors that measure DNA damage. *Current Opinion in Drug Discovery and Development* **2007**, *10*, 67-73.

(26) Hvastkovs, E.; So, M.; Krishnan, S.; Bajrami, B.; Tarun, M.; Jansson, I.; Schenkman, J.; Rusling, J. Electrochemiluminescent arrays for cytochrome P450-activated

genotoxicity screening. DNA damage from benzo[*a*]pyrene metabolites. *Analytical Chemistry* **2007**, *79*, 1897-1906.

(27) Boon, E. M.; Jackson, N. M.; Wightman, M. D.; Kelley, S. O.; Hill, M. G.; Barton, J. K. Intercalative Stacking: A Critical Feature of DNA Charge-Transport Electrochemistry. *The Journal of Physical Chemistry B* **2003**, *107*, 11805-11812.

(28) Jackson, B. A.; Barton, J. K. Recognition of DNA Base Mismatches by a Rhodium Intercalator. *Journal of the American Chemical Society* **1997**, *119*, 12986-12987.

(29) Wong, E. L. S.; Gooding, J. J. Charge Transfer through DNA: A Selective Electrochemical DNA Biosensor. *Analytical Chemistry* **2006**, *78*, 2138-2144.

(30) Wong, E. L. S.; Gooding, J. J. The Electrochemical Monitoring of the Perturbation of Charge Transfer through DNA by Cisplatin. *Journal of the American Chemical Society* **2007**, *129*, 8950-8951.

(31) Hvastkovs, E. G.; Buttry, D. A. Minor Groove Binding of a Novel Tetracationic Diviologen. *Langmuir* **2006**, *22*, 10821-10829.

(32) Hvastkovs, E. G.; Buttry, D. A. Characterization of Mismatched DNA Hybridization via a Redox-Active Diviologen Bound in the PNA-DNA Minor Groove. *Langmuir* **2009**, *25*, 3839-3844.

(33) Krishnan, S.; Hvastkovs, E. G.; Bajrami, B.; Choudhary, D.; Schenkman, J. B.; Rusling, J. F. Synergistic Metabolic Toxicity Screening Using Microsome/DNA Electrochemiluminescent Arrays and Nanoreactors. *Analytical Chemistry* **2008**, *80*, 5279-5285.

(34) Pfeifer, G.; Riggs, A. Genomic sequencing by ligation-mediated PCR. *Molecular Biotechnology* **1996**, *5*, 281-288.

CHAPTER 2: MATERIALS, INSTRUMENTION, AND METHODS

Materials

All DNA oligomer sequences provided in **Table 2.1** were purchased from Integrated DNA Technologies (Coralville, IA).

Table 2.1: DNA oligomer names and their corresponding 21-mer base pair sequences with codons of interest underlined.

Name of Sequence	**Specific Sequence**
wt.273	HS – 5’ – TTT GAG GTG CGT GTT TGT GCC – 3’
wt.273 complement	5’ – GGC ACA AAC ACG CAC CTC AAA – 3’
con.273	HS – 5’ – TTT GAG GTG CCT GTT TGT GCC – 3’
con.273 complement	5’ – GGC ACA AAC AGG CAC CTC AAA – 3’
me.273	HS – 5’ – TTT GAG GTG ^{m}CGT GTT TGT GCC – 3’
me.273 complement	HS – 5’ – GGC ACA AAC ACG CAC CTC AAA – 3’
wt.248.245	HS – 5’ – ATG GGC GGC ATG AAC CGG AGG – 3’
wt.248.245 complement	HS – 5’–CCT CCG GTT CAT GCC GCC CAT – 3’

Benzo[*a*]pyrene-7,8-dihydrodiol-9,10- epoxide, (±)-*anti*-BPDE (BPDE), was obtained from Midwest Research Institute NCI Chemical Carcinogen Reference Standard repository (Kansas City, MO). Benzo[*a*]pyrene (BP), 97% styrene oxide (SO), mercaptohexanol (MCH), tris(hydroxymethyl) aminomethane hydrochloride (Tris-HCl), tris(hydroxymethyl)aminomethane (Tris base), monopotassium phosphate (KH_2PO_4),

dipotassium phosphate (K_2HPO_4), and tetrahydrofuran (THF) were purchased from Sigma-Aldrich. Ammonium acetate used was obtained from Fisher Scientific. Unless stated otherwise, all chemicals were used as received.

Instrumentation

All electrochemical measurements were performed on a CH Instrument 660A workstation (Austin, TX). Potentials were recorded against a saturated Ag/AgCl reference electrode with a platinum wire as the counter electrode and a 2-mm diameter gold (Au) disk

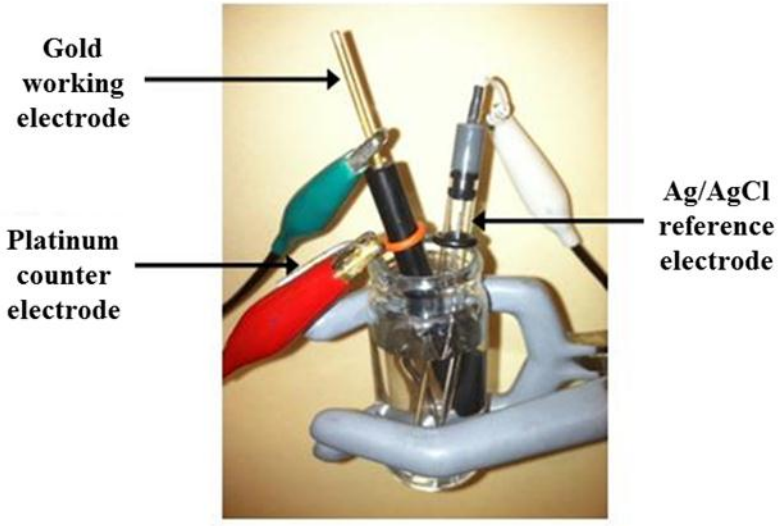

Figure 2.1: The three-electrode electrochemical cell used to perform all electrochemical experiments.

electrode as the working electrode, shown in **Figure 2.1**. The Au electrodes used in this study were purchased from CH Instruments (Austin, Texas) and illustrated in **Figure 2.2**.

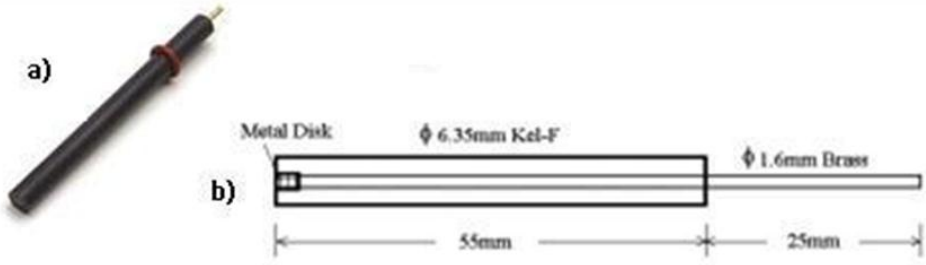

Figure 2.2: a) 2 mm diameter gold disk voltammetry working electrode. b) The dimensions of the CH101 gold working electrode used.

UV-Vis thermal melting experiments were performed on a Varian Cary 300 Bio UV-Vis spectrophotometer with a temperature control unit.

Electrospray ionization mass spectrometry (ESI-MS) experiments were conducted on an Esquire 3000plus quadrupole ion trap mass spectrometer from Bruker Daltonics (Billerica, MA). The instrument has unit mass resolution.

A Nanodrop 2000c Spectrophotometer from Thermo Scientific was used to check and determine the DNA oligomer concentration. Prior to obtaining a concentration reading, a blank was used to acquire a baseline correction absorbance. The DNA sample was then placed on the instrument followed by using preset settings to obtain absorbance values for 260 nm and 280 nm as well as the DNA concentration.

^{1}H NMR measurements were conducted on a Varian 600 MHz spectrometer.

Methods

Buffers

The buffers made and used in this study are listed in **Table 2.2** below.

Table 2.2: A list of buffers used during experimental procedures with each of their corresponding contents and pH level.

Name	**Abbreviation**	**Contents**	**pH**
Electrochemical Buffer	E-Buffer	10 mM Tris 10 mM NaCl	7.4
Hybridization Buffer		10 mM Tris 1 mM EDTA 1 M NaCl	7.4
Immobilization Buffer		1 M Phosphate ($H_2PO_4^-$/HPO_4^{2-}) 1mM EDTA	7.4
Tris-EDTA Buffer	TE Buffer	10 mM Tris 1 mM EDTA	8.0

DNA Preparation for Electrochemical Experiments

ssDNA oligomer sequences for electrochemical studies were purchased with a 5' thiol modification and the complementary oligomers were purchased unmodified. Thiolated oligomers were shipped as disulfides for stability. To reduce the disulfide bonds, 100 μL of 50 mM dithiothreitiol (Sigma) and 2% triethylamine (Sigma) were added to the DNA oligomer and allowed to react at room temperature for 10 min. After 10 min, 500 μL acetone with 2% lithium perchlorate was added to the DNA solution and placed at -20.0°C for 20 min. The DNA solution was then centrifuged at 14,000 x g for 5 min at which point the supernatant was removed. The DNA oligomer pellet was resuspended in TE buffer to make a 1 mM stock solution. Thiolated DNA aliquots were diluted to 1.5 μM with immobilization buffer. Unmodified DNA oligomers were suspended in TE buffer to make a 1 mM stock solution before being diluted to 2.0 μM in hybridization buffer. All DNA was stored at -20.0°C prior to use.

Electrode Preparation

Before DNA experiments, Au electrodes were cleaned following an established protocol to ensure that the Au surface was free from absorbed material and that the electrode was functioning properly.[1] Electrodes were cleaned by submerging in piranha solution (2:1 volume concentrated H_2SO_4 to 30-35% H_2O_2) for 3 to 5 min followed by rinsing with ethanol and deionized water. Electrodes were then polished with 1.0 μm, 0.3 μm, and 0.05 μm diameter alumina particles on a polishing pad (Buehler). Deionized water was used to wet the area with each sequential alumina diameter polish making a slurry. The electrode was passed in a "figure eight" motion through each respective slurry mixture for 2 min each. Following each polish cycle, the electrode was rinsed with deionized water. The electrode was then sonicated for 30 s in deionized water to remove any residual alumina from the electrode surface. Electrodes were

then electrochemically cleaned in 10 mL 0.5 M H_2SO_4 by cycling from 0 V to +1.60 V at 250 mV s^{-1} for approximately 10 min. This was followed by 10 cycles between +0.1 V and +1.43 V at 250 mV s^{-1} to measure the electroactive surface area (quantification cycle). Integration of the Au-oxide stripping wave in the tenth reduction scan of the quantification cycle, illustrated in **Figure 2.3**, was utilized to calculate the actual surface area of the electrode. Integration of the

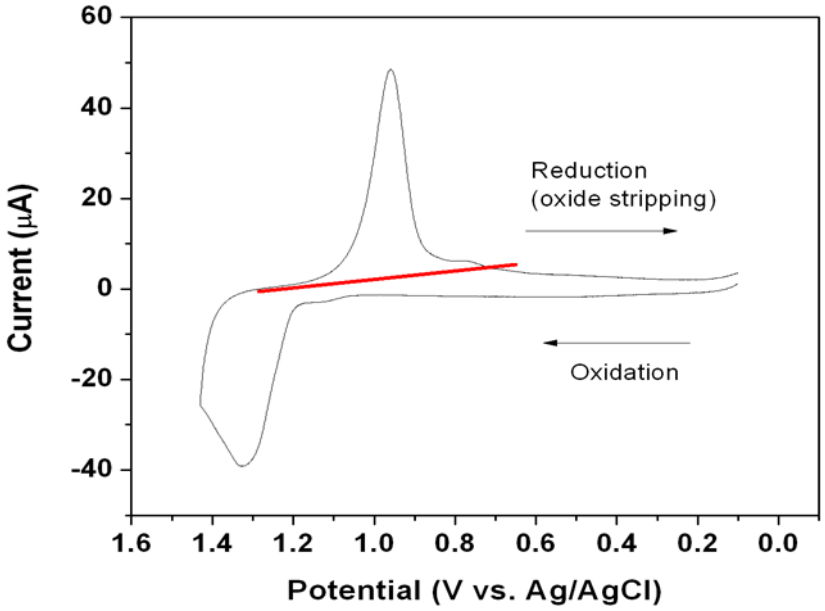

Figure 2.3: Illustration of gold surface quantification cycle that shows integrations of Au-oxide stripping peak using CHI software.

Au-oxide stripping peak provides the charge in Coulombs (C) that can be converted to electrode surface area using the conversion factor 386 μC/cm^2.[2] Typically, this resulted in a surface area of 0.04 cm^2 to 0.05 cm^2 corresponding to a surface roughness factor of 1.3 to 1.6 (calculated as actual surface area/geometrical surface area). The freshly cleaned electrode was immediately removed from the acid, rinsed with ethanol, and then dried under a stream of N_2 or Ar gas.

DNA Immobilization

Cleaned electrodes were exposed to a thiolated ssDNA aliquot for 15 to 30 s. The electrode was rinsed with immobilization buffer and deionized water and then submerged in 5 μM MCH in deionized water for 45 min. MCH acts to passivate the unmodified gold surface and lift non-specifically absorbed ssDNA from the electrode into the solution as shown in **Figure 2.4a**.[3,4] After MCH exposure, the electrode was rinsed with immobilization buffer and was exposed to an unmodified complementary DNA aliquot for 1.5 hr at 37.0°C. The electrode

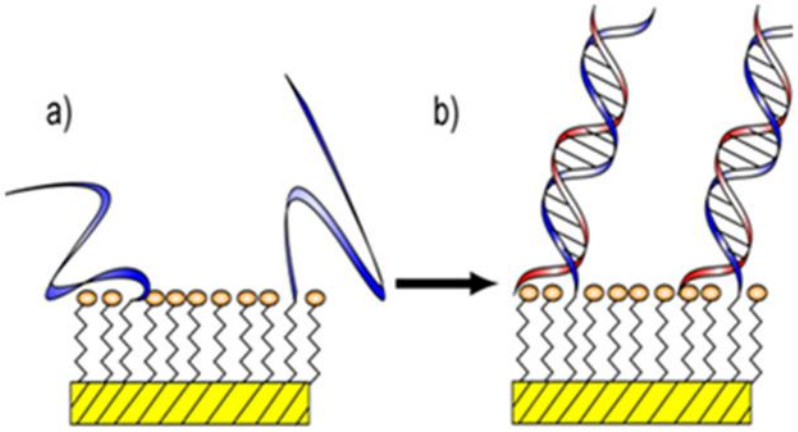

Figure 2.4: Formation of sensor platform. a) ssDNA (blue) is adsorbed on the Au electrode (yellow) by MCH absorption (orange) designed to block bare gold sites. b) Exposure to the complementary sequence (red) results in the formation of dsDNA helices.

was then rinsed with hybridization buffer and immersed in E-buffer for 30 min at 37.0°C to remove non-specifically bound DNA. Newly hybridized electrodes, illustrated in **Figure 2.4b,** were used immediately or stored at 4.0°C prior to use.

Electrochemical Measurements

Voltammetry parameters for different experimental conditions were as follows:

Table 2.3: Cyclic voltammetry parameters for quantification of immobilized DNA.

Initial E	0 V
High E	0 V
Low E	-0.4 V
Final E	0 V
Scan Rate	0.1 V/s
Sweep Segments	4
Sample Interval	0.0001 V
Quiet Time	2 s
Sensitivity	1.00×10^{-6} A/V

Table 2.4: Chronocoulometry parameters for quantification of immobilized DNA.

Initial E	0 V
Final E	-0.4 V
Number of Steps	1
Pulse Width	0.25 s
Sample Interval	0.01 s
Quiet Time	2 s
Sensitivity	1.00×10^{-6} A/V

Table 2.5: Cyclic voltammetry parameters for the detection of C_{12}Viologen and monitoring of DNA Damage from different xenobiotic solutions.

Initial E	0 V
High E	0 V
Low E	-0.7 V
Final E	0 V
Scan Rate	0.1 V/s
Sweep Segments	4
Sample Interval	0.0001 V
Quiet Time	2 s
Sensitivity	1.00×10^{-6} A/V

Table 2.6: Chronocoulometry parameters for detection of C_{12}Viologen and monitoring of DNA Damage from different xenobiotic solutions.

Initial E	0 V
Final E	-0.7 V
Number of Steps	1
Pulse Width	0.25 s
Sample Interval	0.01 s
Quiet Time	2 s
Sensitivity	1.00×10^{-6} A/V

Table 2.7: Square wave voltammetry parameters for detection of C_{12}Viologen and monitoring of DNA Damage from different xenobiotic solutions.

Initial E	-0.20 V
Final E	-0.75 V
Increase E	0.0004 V
Amplitude	0.025 V
Frequency	2 Hz, 5 Hz, or 10 Hz
Quiet Time	2 s
Sensitivity	1.00 x 10^{-6} A/V

Quantification of Immobilized DNA

Prior to DNA damage experiments, the electrode surface density of DNA was calculated according a previously established protocol.[3] The number of DNA probes was assayed by detecting a cationic redox molecule, ruthenium hexamine ($Ru(NH_3)_6$) $^{2+/3+}$, RuHex), that electrostatically binds to the DNA phosphate backbone.[3, 5] The amount of RuHex adsorbed at the DNA-modified electrode was quantified using chronocoulometry (CC). CC measures the charge associated with RuHex reduction, which is related to the absorbed surface coverage by the modified Cottrell equation (**Equation 2.1**).[3]

$$Q = \frac{2nFAD_o^{1/2}C_o^*}{\pi^{1/2}}\, t^{1/2} + Q_{dl} + nFA\Gamma_o \qquad 2.1$$

The variables in **Equation 2.1** are as follows: n is the number of electrons for reduction, F is Faraday's constant, A is the electrode area, D_o is the diffusion coefficient, C_0* is the bulk solution RuHex concentration, Q_{dl} is the capacitive charge and Γ_o is the amount of RuHex at electrode surface (mol cm^{-2}). Plotting Q (obtained from the chronocoulometric measurement) versus $t^{½}$ allows the determination of electroactive charge from diffusing species (first term in **Equation 2.1**), double layer charging (second term in **Equation 2.1**) and surface bound species (third term in **Equation 2.1**).[3] These plots allow one to discern surface bound species from species in the redox solution. This experiment provides the amount of RuHex bound at the electrode interface due to association with DNA.

Equation 2.2 gives the relationship between the surface coverage of RuHex and DNA on the electrode.[3]

$$\Gamma_{DNA} = \Gamma_O \left(\frac{z}{m}\right)(N_A) \qquad 2.2$$

Where Γ_{DNA} is the DNA probe surface density, m is the number of bases in the DNA, z is the charge of redox molecule and N_A is Avogadro's number. The number of DNA bases used in the equation depended on whether or not ssDNA or dsDNA was being quantified. The electrode preparation procedure consistently provided a surface density of dsDNA to be Γ_{DNA} ~1.2 -2.0 x 10^{12} probes of dsDNA per cm^2. Once the Γ_{DNA} was determined, the electrode was submerged into 2 M NaCl for 2 min followed by washing with E-buffer to remove the bound RuHex from the DNA. Lastly, the electrode was placed into an electrochemical cell containing 10 mL of fresh E-buffer.

Synthesis of C_{12}Viologen

The synthesis of an electroactive molecule, $C_{12}H_{25}V^{2+}C_6H_{12}V^{2+}C_{12}H_{25}$ (V^{2+} is 4,4'-bipyridyl or viologen, C_{12}Viologen) followed a previously published procedure which is illustrated in **Figure 2.5**.[1] A di-viologen molecule connected with a hexyl linker was previously synthesized. Approximately 0.20 g of the di-viologen precursor molecule was refluxed in 1 mL DMF and 0.5 mL methanol. Once solubilized, 930 μL 1-bromododecane was added to the flask and allowed to reflux for 24 hr. The yellowish product was dried under vacuum for 4 hr, rinsed with hexane followed by chloroform, and dried under

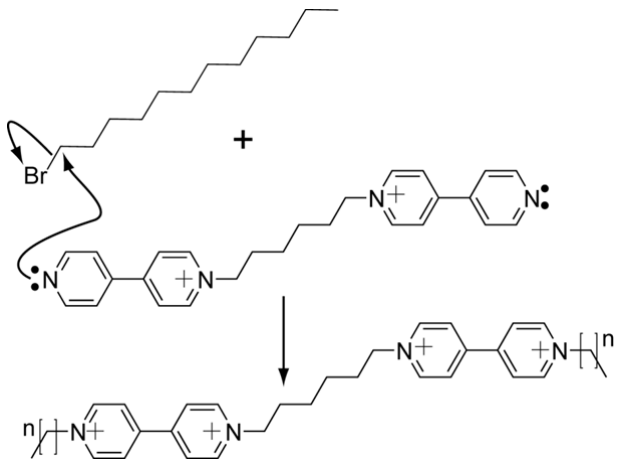

Figure 2.5: Synthesis of C_{12}Viologen from 1-bromododecane and the di-viologen precursor.

vacuum a second time. The C_{12}Viologen product was then recrystallized from ethanol, rinsed with ice-cold ethanol, dried under vacuum, and stored at room temperature until used. The purity of the product was found to be approximately 99% by ^{1}H NMR.

Addition of C_{12}Viologen to Electrochemical Cell

A C_{12}Viologen stock solution was prepared by adding ~0.4 mg to 1.0 mg C_{12}Viologen to 5 mL of E-buffer followed by heating to 45.0°C to solubilize the hydrophobic compound. C_{12}Viologen was added to the electrochemical cell for a final concentration of 9 μM to 11 μM. This concentration was varied depending on voltammetric analysis.

Voltammetric Measurements

The C_{12}Viologen concentration was deemed sufficient if dual wave voltammetry was evident in cyclic voltammetry (CV) and square wave voltammetry (SWV) measurements.[1] Dual wave voltammetry arises from C_{12}Viologen accumulation on dsDNA and is indicative of a properly hybridized electrode, illustrated in **Figure 2.6**.[1, 6] After confirmation of dual wave

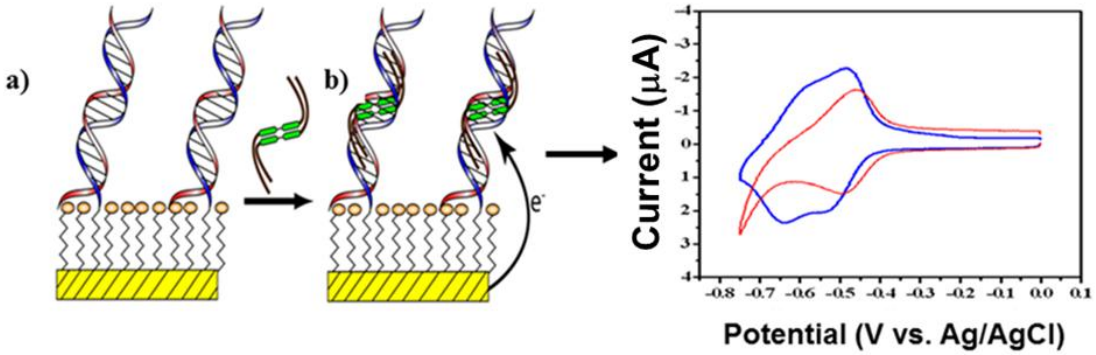

Figure 2.6: Accumulation of C_{12}Viologen in the presence of DNA produces an electrochemical signal. Single wave voltammetry is seen with ssDNA (red) and dual wave voltammetry is seen with dsDNA (blue). Reprinted with permission from Hvastkovs, E. G.; Buttry, D. A. Minor Groove Binding of a Novel Tetracationic Diviologen. *Langmuir* **2006**, *22*, 10821-10829. Copyright 2006 American Chemical Society.

voltammetry, a baseline SWV signal was obtained. This SWV plot was used as a zero minute baseline for timed DNA damage comparison purposes (see below).

BPDE Preparation

BPDE, a known carcinogen, and SO, a suspected carcinogen, both were handled in accordance with the NIH Guidelines for the Laboratory Use of Chemical Carcinogens. The BPDE obtained from NCI Chemical Carcinogen Reference Standards was a racemic mixture of (±)-*anti*-BPDE. BPDE is sensitive to moisture and light conditions; therefore, it was divided into amber vials under N_2 atmosphere. Each individual amber vial was sealed tightly and stored at -20.0°C before use. A 1 mM BPDE stock solution in THF (new fresh stock was used for each experiment) was prepared in the amber vial. THF was stored over molecular sieves prior to use.

SO Preparation

Individual SO solutions (0.5% to 10.0% by volume) were prepared in E-buffer. SO stock solutions were made and used as needed the day of the experiment.

BP Preparation

For each day of electrochemical experiments, a fresh BP stock was prepared. The stock solution was prepared the same day by weighing out BP into an amber vial and solubilizing with THF.

DNA Damage with BPDE

After obtaining the baseline SWV signal the DNA-modified electrode was damaged with BPDE. The electrode was removed from the C_{12}Viologen electrochemical cell and exposed to a 50 μL aliquot containing E-buffer and BPDE of a desired concentration (5.0 μM to 200 μM). The damage reaction was performed at 37.0°C for desired exposure time periods (15-1800 s). Once completed, the electrode was rinsed with E-buffer and placed back into the C_{12}Viologen solution (electrochemical cell). The electrochemical cell was purged with N_2 gas for 5 min prior to voltammetry to remove any oxygen from cell. SWV, CV, and CC were performed using

parameters described previously. Similar protocols were performed for BP and SO damage experiments.

DNA Damage from a Bioactivation Process

To study the effects of bioactivation, DNA-modified electrodes were exposed to BP in the presence of hydrogen peroxide (H_2O_2) and myoglobin (Mb). Similar protocols as previously described were followed. The DNA-modified electrode was exposed to a 500 μL aliquot containing BP (0.1 μM to 50 μM) and 250 nM H_2O_2 in 50 mM phosphate buffer (pH 7.4) at 37.0˚C for desired reaction times. Addition of 3.3 mg mL^{-1} Mb to the reaction medium provided a means to investigate enzymatic bioactivation. Upon completion, the electrode was rinsed with E-buffer and placed back into the electrochemical cell. The cell was then purged with Ar gas for 2 min prior to voltammetry scans. SWV, CV, and CC were conducted using similar protocols.

DNA Preparation for Thermal Melting and Mass Spectrometry Experiments

Unmodified ssDNA oligomers were purchased for ESI-MS and UV-Vis thermal melting experiments. Each ssDNA was resuspended in TE buffer to produce a 1 mM stock solution. Equimolar amounts of each ssDNA were mixed with 50 mM NaCl and heated at 90.0°C for 5 min to produce hybridized dsDNA. The solution was then cooled at room temperature for 5 min. The newly hybridized dsDNA was stored at -20.0°C until used.

Solution Phase DNA Reactions

dsDNA at a concentration of 500 nM was reacted with 1.25 mM BPDE or 2% SO in 50 mM ammonium acetate (pH 6.8) or TE buffer for 1 hr at 4.0˚C in the dark. DNA was removed from the reaction solution by filtering via Millipore 3K 0.5 mL Amicon Ultra Centrifugal filter units for 30 min at 14,000 x g. DNA was rinsed with ammonium acetate buffer and recovered

using the Millipore recommended protocol by inverting the collection filter unit into the recovery tube followed by centrifuging at 1,000 x g for 2 min.

Thermal Melting Studies

Reacted DNA was diluted to 5 μM in ammonium acetate or TE buffer. 50 μL of each sample was pipetted into thermostated quartz cells (Starna Cells, Valencia, CA) and placed into thermal melting UV spectrophotometer. Up to 6 samples could be analyzed simultaneously. Each sample was heated from 35.0ºC to 75.0ºC at a rate of 1.00 ºC/min with a data interval of 0.5ºC.

Electrospray Ionization Mass Spectrometry Studies

Reacted DNA was diluted to 20 μM in 50:50 methanol-water to make 100 μL solution. The solution was injected into the ESI-MS, where each experiment was completed in negative ion mode with a 3 kV potential difference between the emitter and source aperture.

Data Analysis

All of the data was analyzed using OriginPro8 graphing software. CHI voltammetry files were converted to text (.txt) files and imported into Excel. After manipulation in Excel, the spreadsheet was imported into OrginPro8. OriginPro8 was then used for simple arithmetic manipulation of the electrochemical plots including adding/subtracting constants to align the data, baseline (SWV at no damage time) subtractions, peak current measurements, and integration (CV analysis).

References

(1) Hvastkovs, E. G.; Buttry, D. A. Minor Groove Binding of a Novel Tetracationic Diviologen. *Langmuir* **2006**, *22*, 10821-10829.

(2) Bard, A. J.; Faulkner, L. R. In *Electrochemical Methods: Fundamentals and Applications;* Wiley: New York, **2001**.

(3) Steel, A. B.; Herne, T. M.; Tarlov, M. J. Electrochemical Quantitation of DNA Immobilized on Gold. *Analytical Chemistry* **1998**, *70*, 4670-4677.

(4) Herne, T. M.; Tarlov, M. J. Characterization of DNA Probes Immobilized on Gold Surfaces. *Journal of the American Chemical Society* **1997**, *119*, 8916-8920.

(5) Boon, E. M.; Jackson, N. M.; Wightman, M. D.; Kelley, S. O.; Hill, M. G.; Barton, J. K. Intercalative Stacking: A Critical Feature of DNA Charge-Transport Electrochemistry. *The Journal of Physical Chemistry B* **2003**, *107*, 11805-11812.

(6) Hvastkovs, E. G.; Buttry, D. A. Characterization of Mismatched DNA Hybridization via a Redox-Active Diviologen Bound in the PNA-DNA Minor Groove. *Langmuir* **2009**, *25*, 3839-3844.

CHAPTER 3: ELECTROCHEMICAL DETECTION OF ANTI-BENZO[*A*]PYRENE DIOL EPOXIDE DNA DAMAGE AT TP53 CODON 273 OLIGOMERS

Results

Electrochemical Detection of Genotoxicity

Gold electrodes were modified with a 21-mer oligomeric DNA sequence spanning codons 270-276 of the TP53 gene, named wt.273. This particular sequence was used because BPDE is known to adduct DNA at certain guanines in the TP53 gene, primarily at codons 248, 249, and 273.[1] The wt.273 sequence contains the reaction hotspot codon 273 guanine.

Experiments were initially performed to determine whether the sensor was able to detect DNA damage using a redox mediator, C_{12}Viologen. **Figure 3.1a** shows an overview of this type of experiment where BPDE was exposed to the dsDNA sensor. After a desired exposure time, the electrode was rinsed and placed back into an electrochemical cell containing C_{12}Viologen. Genotoxicity detection took place via C_{12}Viologen electrochemical reduction. C_{12}Viologen has been shown to bind selectively to the dsDNA helix.[2] After the DNA-modified electrode was

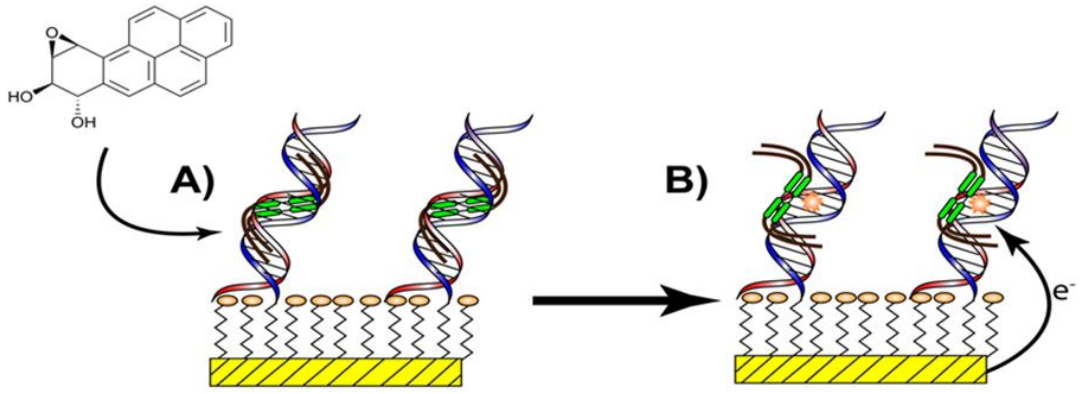

Figure 3.1: A dsDNA electrode a) initially exposed to C_{12}Viologen to obtain a non-damaged DNA signal baseline. b) Exposure to BPDE results in adducted DNA (orange star) altering the binding of C_{12}Viologen (green/brown) to the helix affecting the voltammetric output.

exposed to BPDE, electrochemical measurements were performed to determine the effect of BPDE exposure toward the DNA. It was hypothesized that BPDE damage would distort the helix, altering the binding of C_{12}Viologen to the DNA and its resulting voltammetry. This is illustrated in **Figure 3.1b**.

A standard timed SWV experiment showing C_{12}Viologen voltammetry upon BPDE exposure to wt.273 is shown in **Figure 3.2**. Raw (**Figure 3.2a)** and background subtracted **(Figure 3.2b)** responses were obtained when the wt.273 modified electrode was exposed to 100 μM BPDE for 15 s to 1800 s.

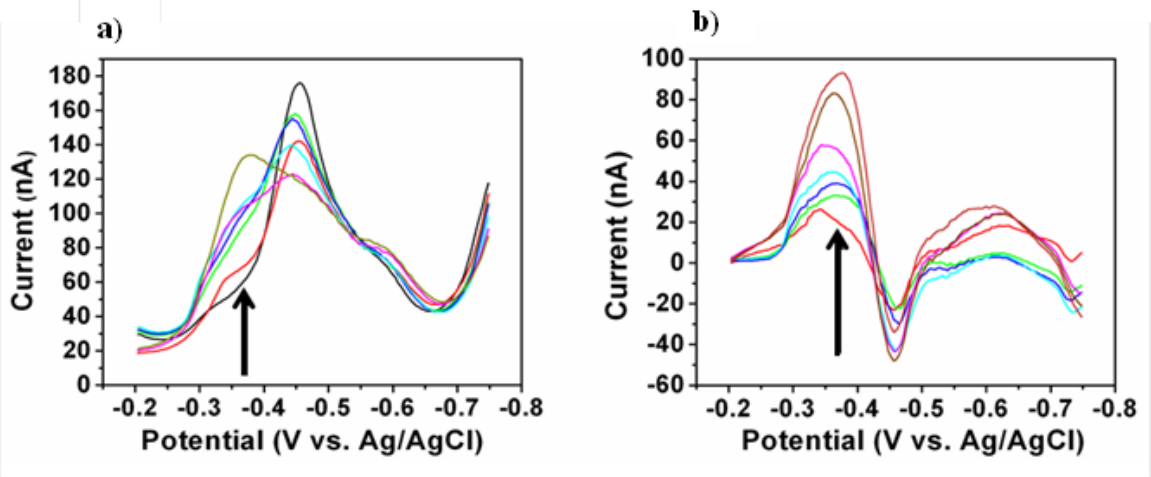

Figure 3.2: a) Raw SWV data obtained for wt.273-modified electrode exposed to 100 μM BPDE for 15 s to 10 min. b) Background subtracted SWV data showing C_{12}Viologen voltammetric changes upon BPDE exposure.

The raw data shows the existence of two bound C_{12}Viologen populations before BPDE exposure, illustrated by dual wave voltammetry (black SWV plot in **Figure 3.2a)**. The first population at approximately -0.46 V is an electrostatic interaction between C_{12}Viologen and DNA and the second population at approximately -0.58 V has been shown to be due to a dimerized C12Viologen bound in the DNA minor groove.[2, 3] Data in **Figure 3.2b** were obtained by subtracting the non-BPDE exposed baseline from each BPDE exposure plot. The background subtracted data shows changes in three bound C_{12}Viologen populations with the emergence of a

new population at -0.37 V, denoted with the arrow in **Figure 3.2**. The positive shifted potential at -0.37 V suggests that the oxidized C_{12}Viologen binds to the DNA with lower free energy. Viologen in this population is more easily reduced than viologen at standard or non-damaged DNA conditions. The origin of the positive shifted peak will be discussed in more detail below.

The magnitude of the peak current at -0.37 V was dependent upon the BPDE concentration, shown in **Figure 3.3a**. After 1 min BPDE exposure to wt.273, the background subtracted SWV signal at -0.37 V increased with increasing BPDE concentration from 10 μM to 200 μM.

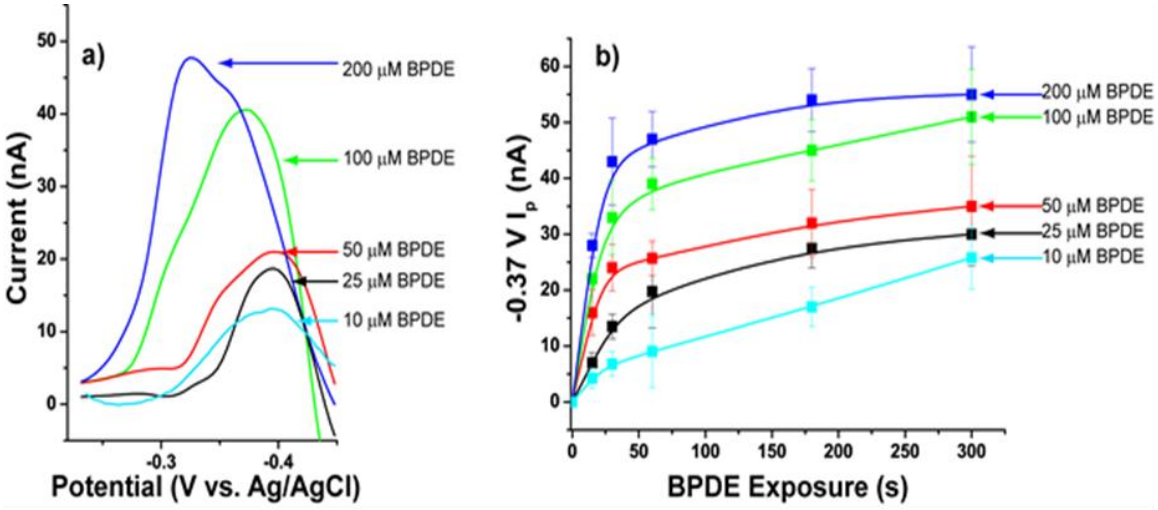

Figure 3.3: a) Background subtracted SWV data at -0.37 V obtained after the wt.273 modified electrode was exposed to denoted BPDE concentrations for 1 min. b) Peak current at -0.37 V plotted versus BPDE exposure time. The error bars represent the average peak current magnitude at -0.37 V per reaction for each concentration.

Figure 3.3a shows that at increasing BPDE concentrations, the -0.37 V peak shifts more positive. This positive shift is evidence of C_{12}Viologen aggregation at the BPDE damage site. We discuss the ramifications of this further below.

The data in **Figure 3.3b** show that the BPDE-DNA reaction is time-dependent and increases at higher BPDE concentrations. This suggests that the BPDE reaction is kinetically

controlled at this DNA sequence. The significance of this will also be discussed in more detail below.

Controls

In order to confirm that the -0.37 V signal was due to BPDE reaction at wt.273, several control experiments were performed. Controls included modifying electrodes with a control DNA sequence where the codon 273 guanine was replaced with a cytosine, named con.273 ("con" = control). Additionally, alternate xenobiotics styrene oxide (SO) and benzo[*a*]pyrene (BP) were exposed to the original codon 273 sequence. **Figure 3.4** shows background subtracted SWV plots comparing these different experimental conditions.

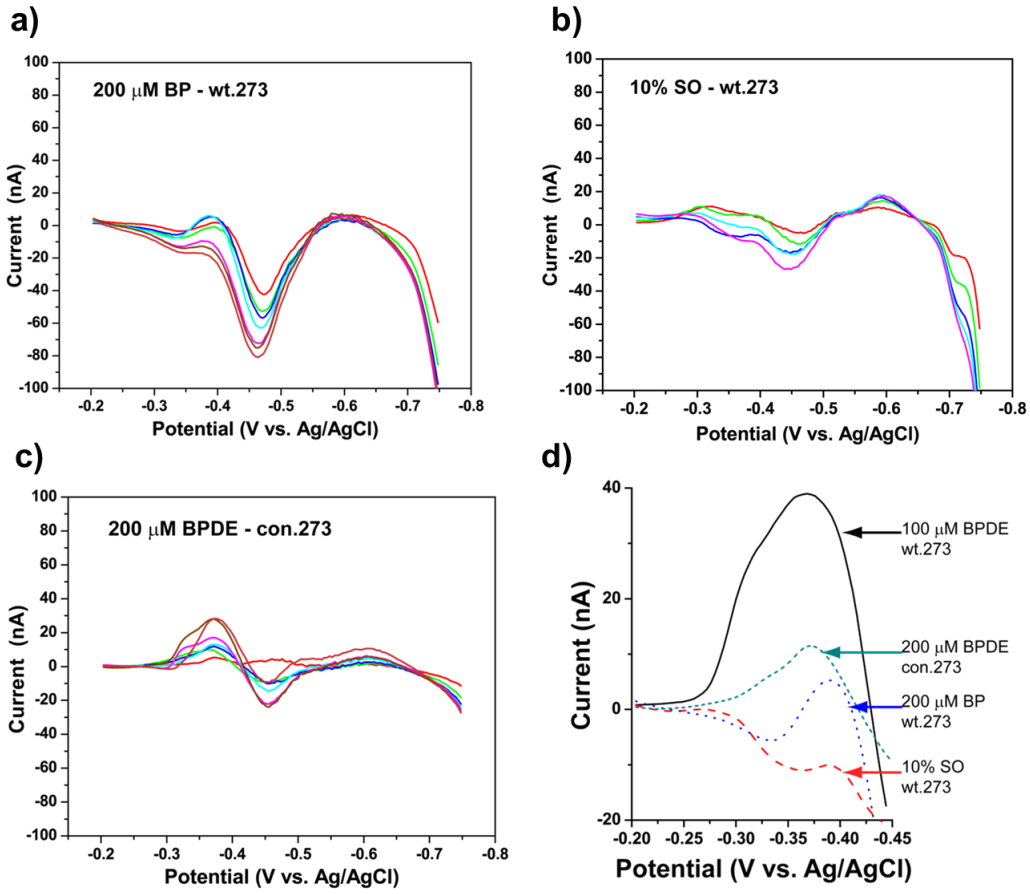

Figure 3.4: Background subtracted SWV data for a) 200 μM BP exposed to wt.273 b) 10% SO exposed to wt.273 c) 200 μM BPDE exposed to con.273 d) Comparing the C_{12}Viologen reduction at -0.37 V for control experiments.

The SWV signal at -0.37 V is dependent upon the DNA sequence and xenobiotic used. Much larger peak currents were seen when BPDE was exposed to wt.273 whereas muted signals were observed when BPDE was exposed to con.273 or when BP or SO were exposed to wt.273. Lower signals obtained when BPDE was exposed to con.273 demonstrate the importance of the codon 273 guanine in wt.273. Also, the muted -0.37 V signal upon SO exposure or nonmetabolized BP demonstrates the sensor is sensitive to BPDE damage. Overall, the control data illustrates the sensor has the ability to detect BPDE-DNA damage at a specific sequence using C_{12}Viologen voltammetry to monitor the damage reaction.

Additional time-dependent studies were conducted to compare wt.273 vs. con.273 exposed to BPDE as well as alternate xenobiotics at wt.273. Initial slopes shown in **Figure 3.5** illustrate that the reaction occurs rapidly when BPDE was exposed to wt.273 and sluggishly at con.273. BP at wt.273 also exhibited very little reaction, which is expected because it lacks reactive functional groups. Overall, these data suggest that the BPDE reaction rate is affected by

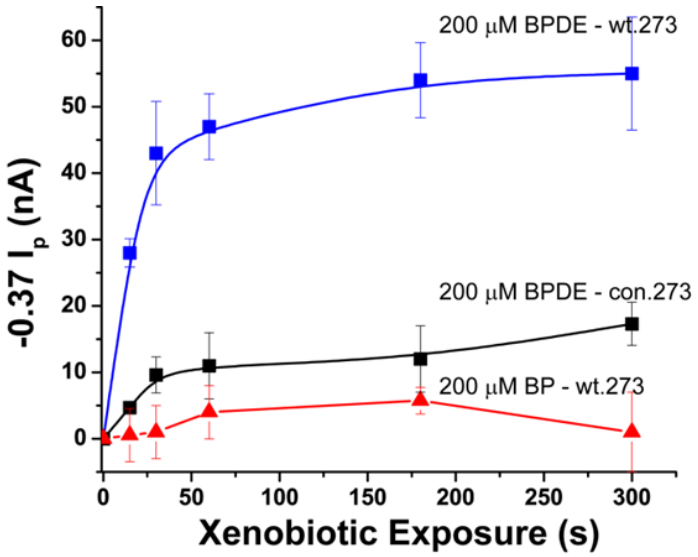

Figure 3.5: Peak current versus xenobiotic exposure time for different experimental conditions. The wt.273 is exposed to 200 μM BPDE (blue) and 200 μM BP (red). The con.273 is exposed to 200 μM BPDE (black).

the presence of guanine. BPDE has been shown to preferentially adduct at guanine sites, and these results support those previous findings.

In order to show that the -0.37 V peak was due to BPDE exposure and not dsDNA dehybridization and subsequent removal from the electrode, a second control experiment using RuHex as redox probe was performed. Data in **Figure 3.6** show RuHex SWV responses when wt.273 was exposed to BPDE from 0 s to 600 s.

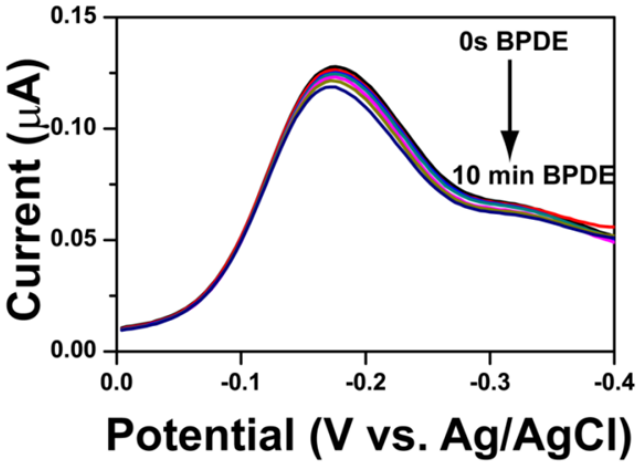

Figure 3.6: The SWV response obtained when the wt.273 was exposed to BPDE for 0 s to 600 s and monitored with $Ru(NH_3)_6^{2+}$, RuHex.

Very small SWV current changes were seen monitoring RuHex reduction upon wt.273 exposure to BPDE. Since very little signal change is seen over the 10 min exposure period, BPDE did not cause significant DNA desorption from the Au electrode. This also provides evidence that C_{12}Viologen voltammetry is based on DNA structural alterations and not a separate desorption or dehybridization process. RuHex is unable to provide DNA structural information because it interacts with DNA solely through electrostatic interactions.[4] This study offers evidence that C_{12}Viologen voltammetry is due to DNA structural alterations.

Thermal Melting Studies

Thermal melting UV-Vis spectrometry provides information pertaining to the xenobiotic-DNA reaction. Thermal melting experiments offer insight on the stability of the dsDNA helix before and after exposure to a xenobiotic.[5] Wt.273 and con.273 DNA sequences were both exposed to BPDE or SO for 60 min followed by filtration techniques to isolate the DNA from the reaction medium. Reacted DNA was heated slowly at a rate of 1˚C/min while monitoring the absorbance at 260 nm. As the temperature increases, the dsDNA duplex denatures due to weakness in hydrogen bonding, which results in dsDNA dehybridization to ssDNA. For a destabilized helix, this transition occurs at lower temperatures. Therefore, this technique offers the means to assay the helix stability based on xenobiotic exposure. **Figure 3.7** shows typical DNA thermal profiles. **Figure 3.7a** shows wt.273 in ammonium acetate buffer either unexposed (red) or exposed (black) to BPDE while **Figure 3.7b** shows the same for con.273. The melting transition (T_m) occurs when the normalized 260 nm absorbance is at approximately 0.5 (where ssDNA and dsDNA exist in a 50/50 ratio). The difference in T_m (ΔT_m) provides a measure of induced DNA helical instability caused by xenobiotic exposure.[5] Additionally, the slope of

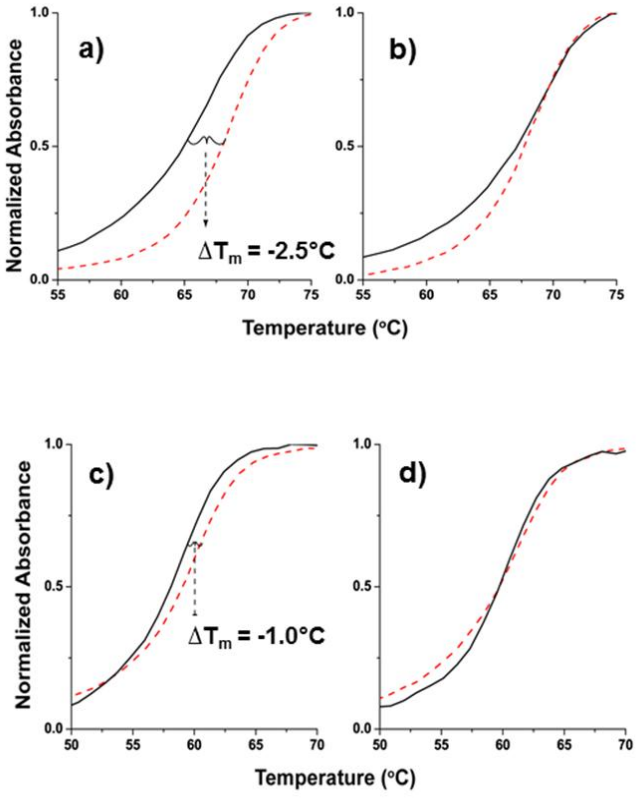

Figure 3.7: Thermal melting profiles of DNA not exposed (red) or exposed (black) to BPDE (a) wt.273 and (b) con.273 in ammonium acetate buffer or (c) wt.273 and (d) con.273 in E-Buffer.

the transition is indicative of the helix stability.[5] Melting curves showing a rapid transition between dsDNA and ssDNA indicate more stable dsDNA, whereas a more drawn out transition denotes instability.[5] Thermal profiles obtained for BPDE exposed to wt.273 using ammonium acetate buffer exhibited ΔT_m of -2.5 ± 0.1 ˚C (**Figure 3.7a**). Using E-Buffer, the ΔT_m was -1.0 ± 0.1˚C (**Figure 3.7c**). Smaller ΔT_m illustrates that the wt.273 did not react as well with BPDE in E-Buffer, presumably due to the BPDE reaction with the Tris (2-Amino-2-hydroxymethyl-propane-1,3-diol) component, which exhibits an amine functional group. ΔT_m obtained when BPDE was exposed to con.273 in ammonium acetate (**Figure 3.7b**) or E-Buffer (**Figure 3.7d**) showed muted ΔT_m decreases compared to wt.273. Overall, the larger ΔT_m for wt.273 oligomers exposed to BPDE in conjunction with the gradual dsDNA-ssDNA melting transition denote more wt.273 instability after BPDE exposure vs. con.273.

An additional control was conducted by exposing wt.273 to SO. SO exposure to wt.273 resulted in negligible ΔT_m, shown in **Figure 3.8**. This demonstrates that SO adducts do not affect DNA stability. SO is known to adduct DNA at different guanine locations and orient in a different manner than BPDE. The SO binding locations and orientations do not cause major

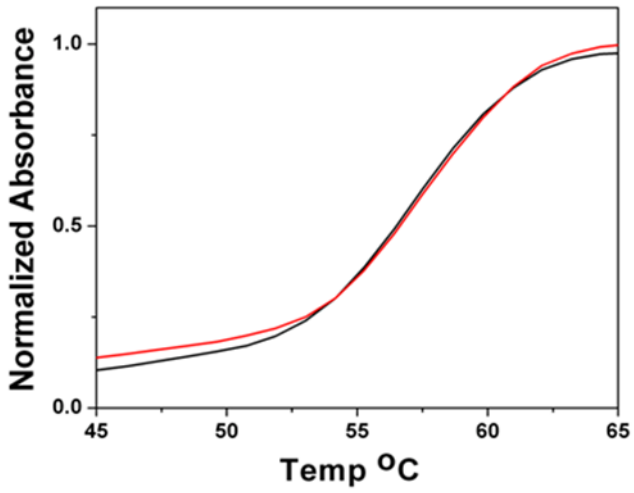

Figure 3.8: Thermal melting curve obtained when wt.273 was exposed to 2% SO

DNA sequence disruptions, which results in unchanged thermal melting profiles seen in **Figure 3.8**. This is discussed in more detail below. Overall, the representative thermal melting profiles provided are consistent with electrochemical responses obtained when wt.273 was exposed to BPDE.

Mass Spectrometry Studies

Mass spectrometry was performed to determine the number of adducts per DNA duplex after xenobiotic exposure, and provide insight into the BPDE-DNA reaction. Representative mass spectra are shown in **Figure 3.9**. **Figure 3.9a** shows wt.273 exposed to BPDE. ESI conditions result in dsDNA dehybridization; therefore, the spectra show m/z charge states for individual ssDNA along with sodium adduction. This can be seen in the expanded view of **Figure 3.9a.** Here, the spectrum shows the presence of four distinct species. Peaks at m/z 635

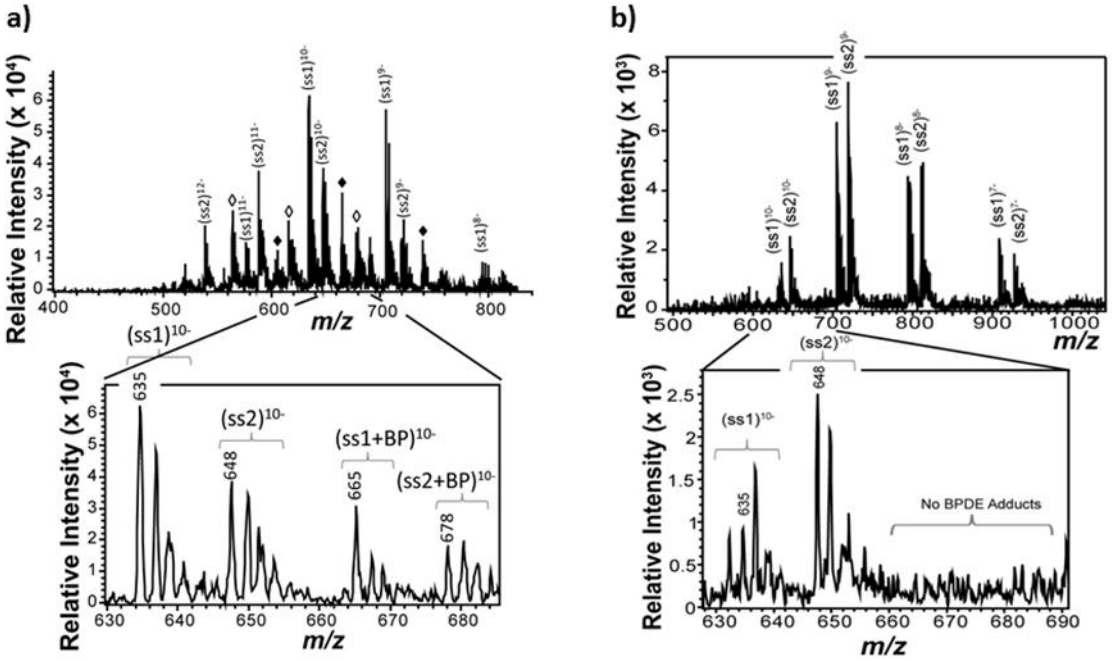

Figure 3.9: Mass spectra showing the charge states a) detected when BPDE was exposed to wt.273. ss1 singly adducted with BPDE is denoted by black diamond (♦). ss2 singly adducted with BPDE is denoted by open diamond (◊). b) Wt.273 exposed to similar conditions as a) but without BPDE exposure. In the expanded view of m/z 630-685 shows the 10- charge state and sodium adduction.

and 648 represent the individual unreacted ssDNA that make up wt.273 dsDNA, termed ss1 and ss2 respectively. Peaks at m/z 665 and 678 represent ss1 and ss2 each with a single BPDE adduct. **Figure 3.9b** shows a control experiment conducted under similar experimental conditions without BPDE. The spectrum shows only two unreacted ssDNA species and no BPDE adducted ssDNA.

Figure 3.10 shows mass spectra for individual ssDNA exposed to BPDE. These spectra show evidence of mainly singly and some doubly BPDE-adducted oligomers suggesting that even as freely accessible unhybridized oligomers, each reactive site, most likely guanine sites, does not equally react with BPDE. The MS results can be interpreted in one of two different ways. One is the formation of a single adduct on either ss1 *or* ss2 per dsDNA. The other possibility is the formation of one BPDE adduct on each ssDNA or two BPDE adducts per duplex. The mass spectra show that only a discrete number of DNA adducts form on the DNA, which is hybridized prior to ESI exposure, based on previously discussed thermal melting data. Additionally, spectra show that ssDNA does not readily adduct BPDE despite the more accessible structure. Taken together, this likely suggests that a single adduct forms on each dsDNA, and upon dehybridization in the ESI, this results in one unreacted and one BPDE-adducted

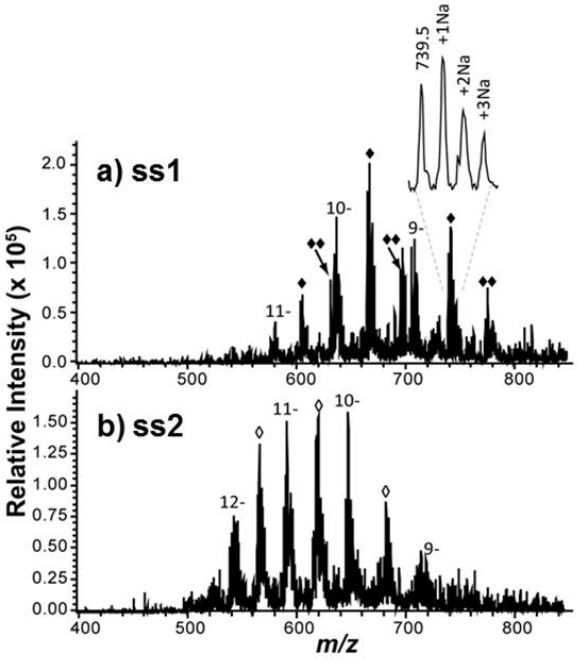

Figure 3.10: Mass spectra showing the charge state distribution with BPDE being exposed to a) ss1 and b) ss2, which are the individual ssDNA making up the wt.273 sequence. The black diamonds represent BPDE adduction to ss1 either singly adducted (♦) or doubly adducted (♦♦). The single adducts on ss2 are denoted by open diamonds (◊). The inset shows Na^+ adduction that accounts for the spectral complexity of spectra.

ssDNA. If two BPDE adducts were formed on the dsDNA helix, the short 21-mer sequence would likely be very unstable resulting in larger ΔT_m values in thermal melting analysis.

Mass spectra were also obtained for BPDE exposed to con.273 as a comparison to the wt.273 results. The spectrum in **Figure 3.11** shows predominantly unreacted ssDNA when con.273 was exposed to BPDE. Low levels of BPDE adducted ssDNA demonstrates that the BPDE reaction did not occur with the same efficiency as at wt.273. Since the only difference in the two DNA sequences is the substitution of guanine with cytosine in con.273, this data provides evidence that the codon 273 guanine in wt.273 is likely the main BPDE adduct site. In addition, con.273 thermal melting profiles showed only slight ΔT_m changes denoting very little helical destabilization.

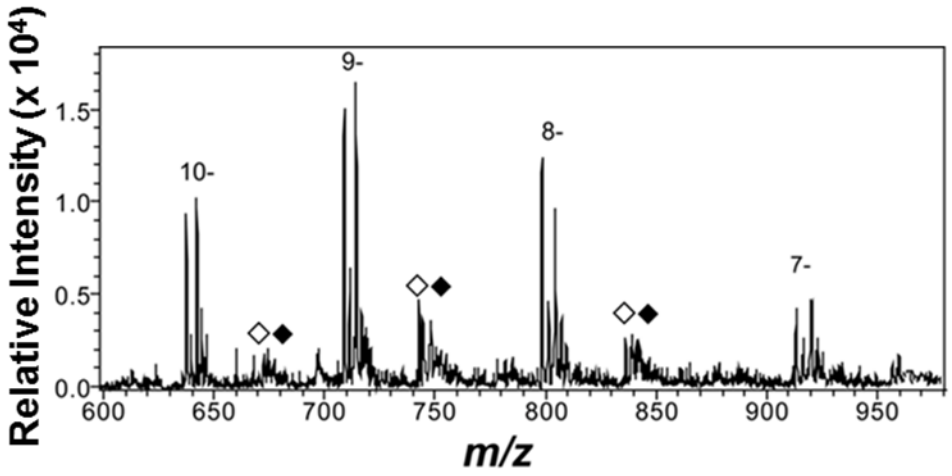

Figure 3.11: Mass spectra showing the charge distrubtion after con.273 had been exposed to BPDE.

Figure 3.12 shows a spectrum where wt.273 was exposed to SO. **Figure 3.12** shows m/z values that are consistent with both ss1 and ss2 being adducted by SO to produce two SO adducts per DNA duplex. Additionally, some hybridized dsDNA with two SO adducts are seen in the spectrum. This spectrum shows that SO does adduct the dsDNA. Therefore, the lack ΔT_m

or electrochemical signal seen upon SO exposure most likely resulted from the lack of SO-induced DNA destabilization rather than a sluggish reaction at DNA.

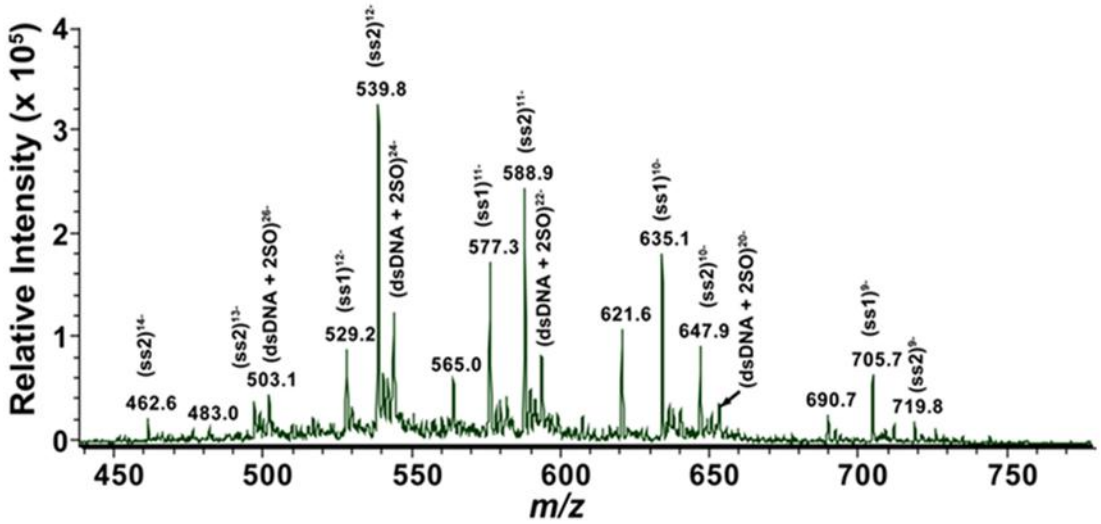

Figure 3.12: Mass spectra showing the charge states detected when wt.273 was exposed to SO.[6] The data obtained shows that SO can form a discrete number of adducts, like BPDE. In particular this study provided evidence that SO adducts are forming but our electrochemical platform can sensitively detect sequence specific damage as well as specific adduct types

Overall, the mass spectra and thermal melting profiles provide evidence that the reaction exhibits a degree of specificity for a particular guanine in the codon 273 sequence. These data also are consistent with the electrochemical sensor data where obtained signals were much higher in cases where BPDE reacted at wt.273. Overall, thermal melting and MS experiments provide a degree of validation for the electrochemical sensor response.

Discussion

Electrochemical monitoring of DNA immobilized on Au electrodes after BPDE exposure showed changes in three bound C_{12}Viologen populations where a new lower energy bound population was observed at -0.37 V. The emergence of this new peak suggests that the BPDE reaction affects the DNA helix and alters the C_{12}Viologen binding environment. C_{12}Viologen voltammetry is influenced by the dsDNA structure.[2, 3] The initial SWV voltammograms (**Figure 3.2a**) before BPDE exposure showed two C_{12}Viologen populations. The negative

shifted population at -0.58 V has been shown to be due to a dimerized form bound on the dsDNA. The dimer results when two singly-reduced cation radical viologen ($V^{\bullet+}$) species overlap their singly occupied π^* orbitals.[7] The population at -0.45 V has been shown to be due to an electrostatic interaction between the cationic viologen and the anionic DNA backbone. The reaction with BPDE slightly changes the binding environments of these two bound forms, while introducing a new lower energy bound population. In order to understand this process, a brief discussion on BPDE stereochemistry is necessary.

Through metabolism processes, BPDE can become one of four different stereoisomers, and the stereochemistry plays a critical role in its eventual mutagenicity.[8, 9] The four possible BPDE stereoisomers are shown in **Figure 3.13**.

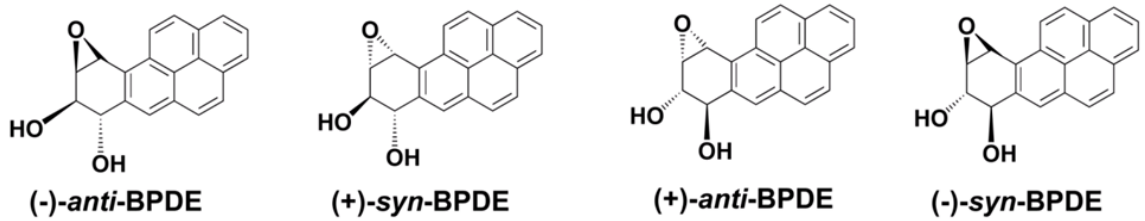

Figure 3.13: Four BPDE stereoisomers.

A racemic (±)-*anti*-BPDE sample was utilized in these experiments. These two compounds will react differently at DNA.[8-10] Nucleophilic guanine amine sites in DNA will

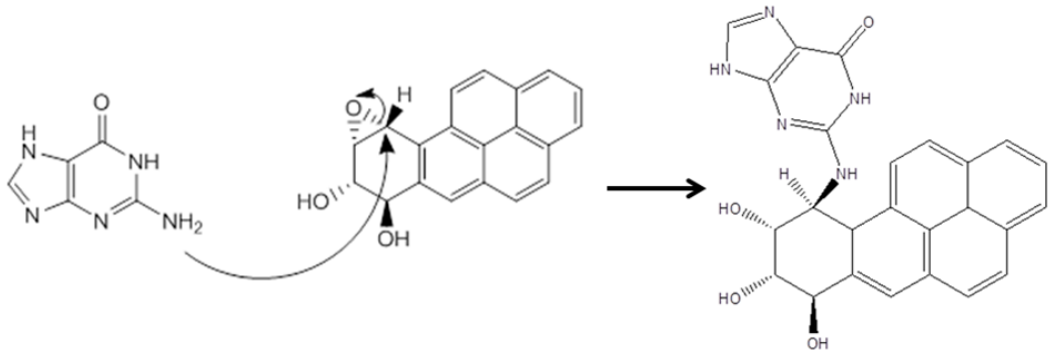

Figure 3.14: An S_N2 reaction is illustrated, where electrophilic BPDE is attacked by the nucleophilic guanine N^2 amine causing a *trans* covalent adduct.

attack electrophilic BPDE through an S_N2 mechanism.[9] This reaction is shown in **Figure 3.14**. Typically, BPDE reacts at the exocyclic amine N^2 positions of the guanine base.[9, 11]

When a BPDE enantiomer adducts guanine it gives rise to two possible adducts with different configurations, demonstrated in **Figure 3.15**.[10] These reactions do not produce an equal product spectrum, however. Previous work has shown that when the different BPDE enantiomers are exposed to similar DNA as used in this study, the expected product distribution is highly dependent on the particular enantiomer involved.[10] The expected percentage of products is also shown in **Figure 3.15**.[10] For instance, when (+)-*anti*-BPDE is exposed to DNA, the (+)-*trans*-*anti*-[BP]-N^2-guanine product will be expected 94% of the time.[10]

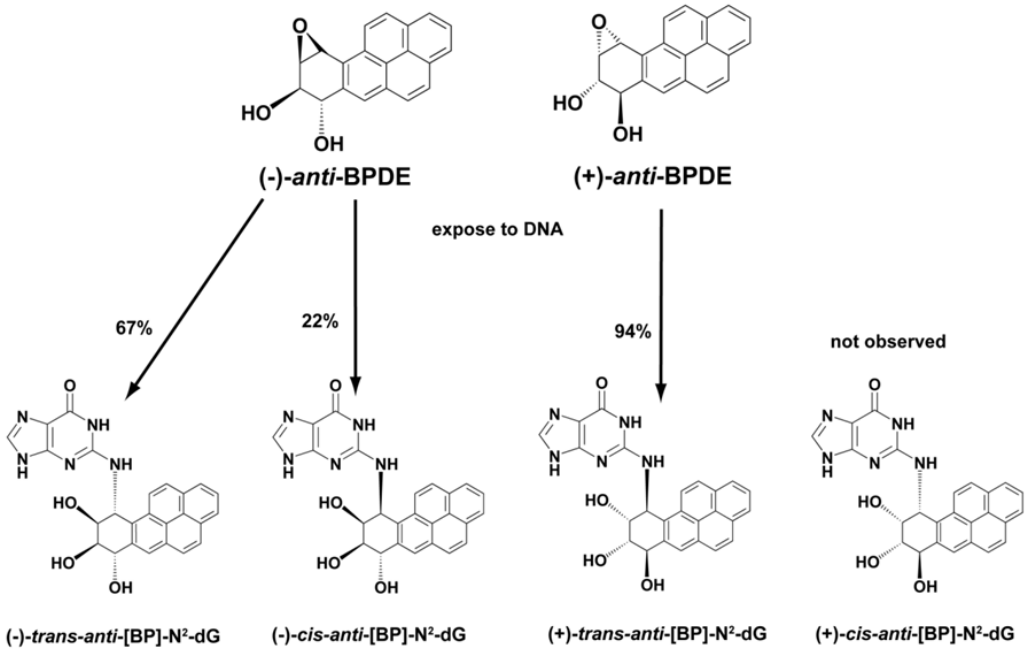

Figure 3.15: The racemic mixture of BPDE exposed to DNA gave rise to two different adducts with different configurations per enantiomer.

Guanine adduct stereochemistry affects how the bulky BPDE adduct orients within the dsDNA duplex.[10,9] (+)-*trans* and (-)-*trans*-BPDE adducts align within the minor groove of DNA with the edge of the pyrenyl moiety exposed to external solution.[10, 12] This alignment of the BPDE pyrenyl ring results in minimal minor groove base-pairing disruptions. Pyrene at this

location accesses the aqueous exterior of DNA, which is unfavorable from a free energy standpoint, but this is a trade-off to ensure the retention of Watson-Crick base-pairing.[9, 10] These adducts are shown in **Figure 3.16**. (-)-*cis*-BPDE adducts result in an intercalating BPDE that forces the adducted guanine into the minor groove while displacing the opposite cytosine base pair into the major groove.[10,8] Low amounts of BP-adenine adducts are also expected, which provides the remainder of the product spectrum.

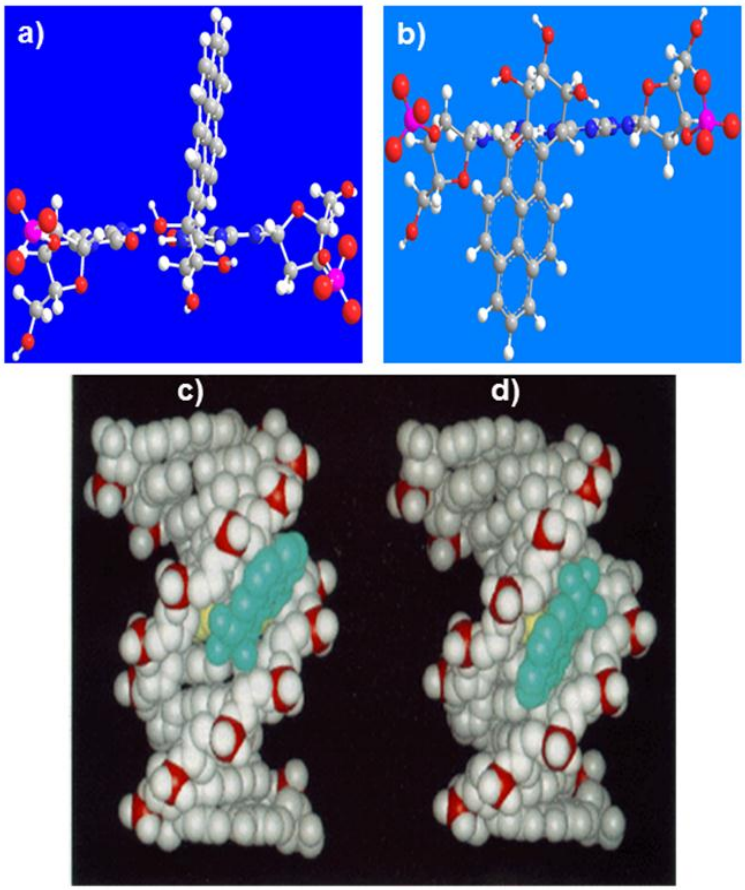

Figure 3.16: Three-dimensional ball and stick model of C-G base pair looking into the minor groove a) (+)-*trans-anti*-BPDE adducts guanine and angles toward 5' direction of modified strand and b) (-)-*trans-anti*-BPDE adducts guanine angles toward 3' direction of modified strand. Space-filling model c) (+)-*trans-anti*-BPDE adduct has pyrenyl ring (cyan) oriented toward 5' direction of modified strand in minor groove and d) (-)-*trans-anti*-BPDE adduct has pyrenyl ring oriented toward 3' direction of modified strand in minor groove. c) and d) Reprinted with permission from Geacintov, N.; Cosman, M.; Hingerty, B.; Amin, S.; Broyde, S.; Patel, D. NMR solution structures of stereoisomeric covalent polycyclic aromatic carcinogen-DNA adduct: principles, patterns, and diversity. *Chem. Res. Toxicol.* **1997**, *10*, 111-146. Copyright 1997 American Chemical Society.

Under the experimental conditions described here, the racemic BPDE mixture means that DNA was exposed to approximately a 50/50 ratio of (+)-*anti*-BPDE and (-)-*anti*-BPDE. (+)-*anti*-BPDE exposure to wt.273 will result almost exclusively in minor groove oriented BPDE adducts aligned in the 5' direction of the modified strand, as demonstrated in **Figure 3.16c**.[10, 12] (-)-*anti*-BPDE exposure to the wt.273 will result in minor groove oriented BPDE adducts aligned in the 3' direction of the modified strand, as shown in **Figure 3.16d**, as well as some intercalating species.[10, 12] This split between minor groove bound and intercalated BPDE from (-)-*trans*-BPDE would be expected to occur in an approximate 70/30 ratio. Overall, the majority of expected wt.273 products from (±)-anti-BPDE exposure will be minor groove aligned *trans*-[BP]-guanine adducts, with a small amount of intercalating species.

Because the pyrenyl moiety is accessible to the aqueous exterior, the resulting minor groove aligned BPDE adducts will provide an external hydrophobic site on the DNA helix. This site will promote favorable hydrophobic interactions between BPDE and alkyl C_{12}Viologen moieties. At sufficiently elevated C_{12}Viologen concentrations, this will cause an aggregation of C_{12}Viologen, and dimerization upon reduction to the $V^{\bullet+}$ cation radical viologen form.[7] The formal reduction potential (E^{f}_{red}) of C_{12}Viologen is approximately -0.45 V. The positive shift in reduction (-0.37 V, approximately 80 mV) denotes that the oxidized C_{12}Viologen form is less stable and driving force exists for reduction to the cation radical form. Overlap of singly occupied π^{*} orbitals provides this driving force – i.e., the $V^{\bullet+}$ π dimer is more stable. Additionally, the positive shift is more dramatic at higher BPDE concentrations (**Figure 3.3a**). This may be due to the higher degree of minor groove BPDE adducts facilitating viologen aggregation and dimerization.

Concerning the changes in the other bound forms (-0.45 and -0.55 V), these can be explained by the small percentage of intercalating (-)-*cis*-*anti*-[BP] guanine adducts that intercalate into the dsDNA helix. Here, an increase in the signal at -0.55 V is seen denoting additional C_{12}Viologen bound in this population. This population was previously assigned to π-dimers bound in the minor groove. Hydrophobic interactions between the minor groove and the alkyl C_{12}Viologen regions promote aggregation and dimerization upon reduction.[7] As the bulky BPDE displaces the adducted guanine into the minor groove, this presumably increases these hydrophobic interactions, facilitating additional C_{12}Viologen binding at this locale. Some stretching of the DNA helix through the intercalation could account for the subsequent loss of the electrostatic bound (-0.45 V) viologen. Bulky minor groove bound BPDE adducts may also displace this C_{12}Viologen population as well.

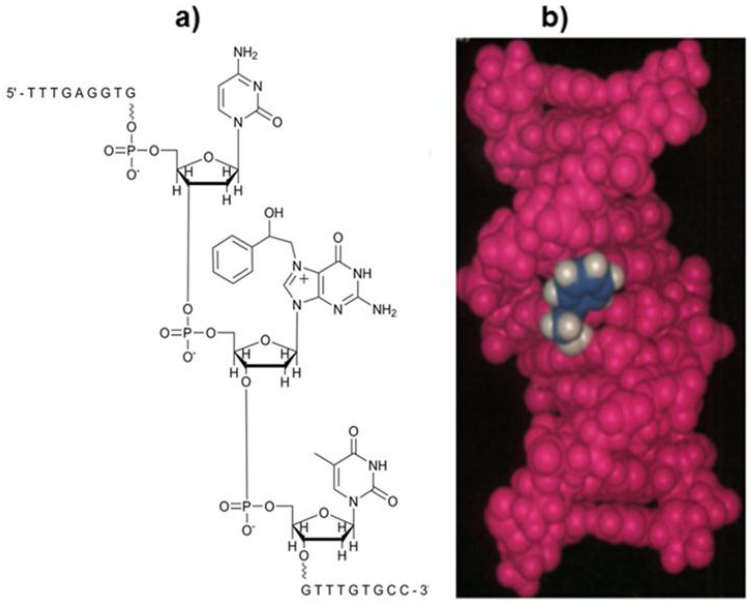

Figure 3.17: a) SO covalently adducted at the N7 guanine position b) Space filling model of a SO adduct oriented in the 5' direction toward modified strand occupying the major groove. Reprinted with permission from Feng, B.; Voehler, M.; Zhou, L.; Passarelli, M.; Harris, C. M.; Harris, T. M.; Stone, M. P. Major Groove (S)-a-(N6-Adenyl)styrene Oxide Adducts in an Oligodeoxynucleotide Containing the Human N-ras Codon 61 Sequence: Conformations of the S(61,2) and S(61,3) Sequence Isomers from 1H NMR . *Biochemistry (N. Y.)* **1996**, *35*, 7316-7329. Copyright 1996 American Chemical Society.

Control experiments using con.273 revealed muted or no emergence of the -0.37 V peak. This suggests that the central codon 273 guanine is the main BPDE adduct location in wt.273. Experiments with alternate xenobiotics BP and SO showed that no -0.37 V peak was seen. The lack of positive shifted potential denotes that these

xenobiotics do not produce an external, minor groove adduct. The majority of SO adducts are guanine N7 adducts aligned in the major groove.[11] This is seen in **Figure 3.17**. Adducts at these locations presumably do not promote C_{12}Viologen aggregation, or the SO adduct is not sufficiently hydrophobic to promote aggregation at this site.

BP exposure did cause a large decrease at -0.45 V. Nonmetabolized BP is known to intercalate within the base pairs of DNA causing base pair bulging and helical elongation with slight unwinding.[13-15] The decrease at -0.45 V is presumably due to elongation of the DNA helix, which alters the spacing of negatively charged phosphates and impacts the alignment of cationic C_{12}Viologen along the phosphate backbone. By changing the spacing, the electrostatic binding of C_{12}Viologen to the helix is more unfavorable.

Overall, the electrochemical and spectroscopic data are consistent with sequence-specific DNA damage detection, with solid evidence toward site-specific DNA damage detection at the codon 273 guanine. An extensive research effort has shown that BPDE reacts at DNA based on sequence effects. Data provided show that BPDE reacts preferentially at the 5'-CpG-3' sequences. BPDE stereochemistry producing an array of DNA-adducts in conjunction with C_{12}Viologen redox chemistry explains the unique voltammetric responses upon electrochemical analysis.

References

(1) Denissenko, M. F.; Pao, A.; Tang, M.; Pfeifer, G. P. Preferential Formation of Benzo[a]pyrene Adducts at Lung Cancer Mutational Hotspots in P53. *Science* **1996**, *274*, 430-432.

(2) Hvastkovs, E. G.; Buttry, D. A. Minor Groove Binding of a Novel Tetracationic Diviologen. *Langmuir* **2006**, *22*, 10821-10829.

(3) Hvastkovs, E. G.; Buttry, D. A. Characterization of Mismatched DNA Hybridization via a Redox-Active Diviologen Bound in the PNA-DNA Minor Groove. *Langmuir* **2009**, *25*, 3839-3844.

(4) Steel, A. B.; Herne, T. M.; Tarlov, M. J. Electrochemical Quantitation of DNA Immobilized on Gold. *Analytical Chemistry* **1998**, *70*, 4670-4677.

(5) Mergny, J.; Lacroix, L. Analysis of Thermal Melting Curves. *Oligonucleotides* **2003**, *13*, 515-537.

(6) Satterwhite, J. E.; Pugh, A. M.; Danell, A. S.; Hvastkovs, E. G. Electrochemical Detection of anti-Benzo[*a*]pyrene Diol Epoxide DNA Damage on TP53 Codon 273 Oligomers. *Analytical Chemistry* **2011**, *83*, 3327-3335.

(7) Tang, X.; Schneider, T. W.; Walker, J. W.; Buttry, D. A. Dimerized-Complexes in Self-Assembled Monolayers Containing Viologens: An Origin of Unusual Wave Shapes in the Voltammetry of Monolayers. *Langmuir* **1996**, *12*, 5921-5933.

(8) Kozack, R.; Seo, K.; Jelinsky, S. A.; Loechler, E. L. Toward an understanding of the role of DNA adduct conformation in defining mutagenic mechanism based on studies of the major adduct (formed at N2-dG) of the potent environmental carcinogen, benzo[a]pyrene. *Mutation Research/Fundamental and Molecular Mechanisms of Mutagenesis* **2000**, *450*, 41-59.

(9) Huetz, P.; Poux, V. Carcinogenicity of benzo[*a*]pyrene diol epoxide stereoisomers: A linear free energy relationship study. *Journal of Molecular Structure* **2006**, *764*, 167-176.

(10) Geacintov, N.; Cosman, M.; Hingerty, B.; Amin, S.; Broyde, S.; Patel, D. NMR solution structures of stereoisometric covalent polycyclic aromatic carcinogen-DNA adduct: principles, patterns, and diversity. *Chemical Research of Toxicology* **1997**, *10*, 111-146.

(11) Hemminki, K.; Försti, A.; Mustonen, R.; Savela, K. DNA adducts in experimental cancer research. *Journal of Cancer Research and Clinical Oncology* **1986**, *112*, 181-188.

(12) Xie, X.; Geacintov, N. E.; Broyde, S. Stereochemical Origin of Opposite Orientations in DNA Adducts Derived from Enantiomeric anti-Benzo[*a*]pyrene Diol Epoxides with Different Tumorigenic Potentials. *Biochemistry (N. Y.)* **1999**, *38*, 2956-2968.

(13) Geacintov, N. E.; Prusik, T.; Khosrofian, J. M. Properties of Benzopyrene-DNA Complexes Investigated by Fluorescence and Triplet Flash Photolysis Techniques. *Journal of the American Chemical Society* **1976**, *98*, 6444-6452.

(14) Meehan, T.; Gamper, H.; Becker, J. F. Characterization of reversible, physical binding of benzo[a]pyrene derivatives to DNA. *The Journal of Biological Chemistry* **1982**, *257*, 10479-10485.

(15) Boyland, E.; Green, B. The interaction of polycyclic hydrocarbons and nucleic acids. *British Journal of Cancer*. **1962**, 507-517.

CHAPTER 4: CYTOSINE METHYLATION INFLUENCE ON THE ELECTROCHEMICAL DETECTION OF DNA DAMAGE FROM BENZO[*A*]PYRENE DIOL EPOXIDE

Results

Electrochemical Detection

Gold electrodes were modified with methylated sequence dsDNA oligomers (named me.273 from here on). Me.273 exhibits the same 21-mer sequence as wt.273 except that the codon 273 cytosine 5' to guanine on the probe ssDNA was methylated at the 5-carbon (**Figure 4.1**). A large percentage of the CpG sites in the human genome contain 5-methylcytosine.[1] In addition, studies have demonstrated that the reactivity of BPDE with guanine was strongly impacted by cytosine methylation.[2-4]

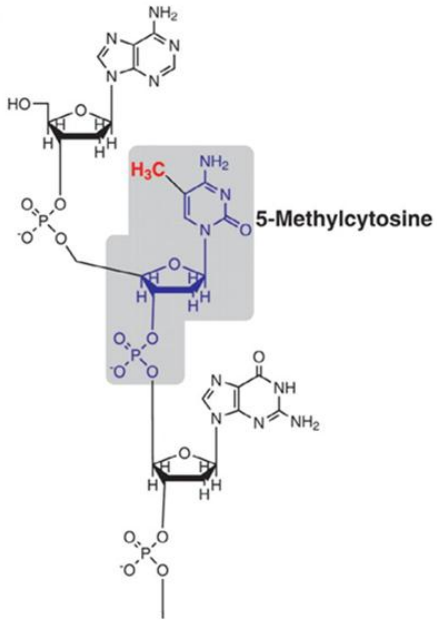

Figure 4.1: Cytosine is methylated at the 5-carbon, named 5-methylcytosine

Similar experiments were performed as outlined in Chapter 3 in order to determine the effects of cytosine methylation on the sensor response. It was hypothesized that the electrochemical response may be influenced in some way by the epigenetic modification.

Figure 4.2 shows background subtracted SWV responses comparing me.273 and wt.273 electrodes exposed to 100 μM BPDE from 15-600 s. The figure shows that the electrochemical response at me.273 is much different than at wt.273. In addition, to the emergence of the peak

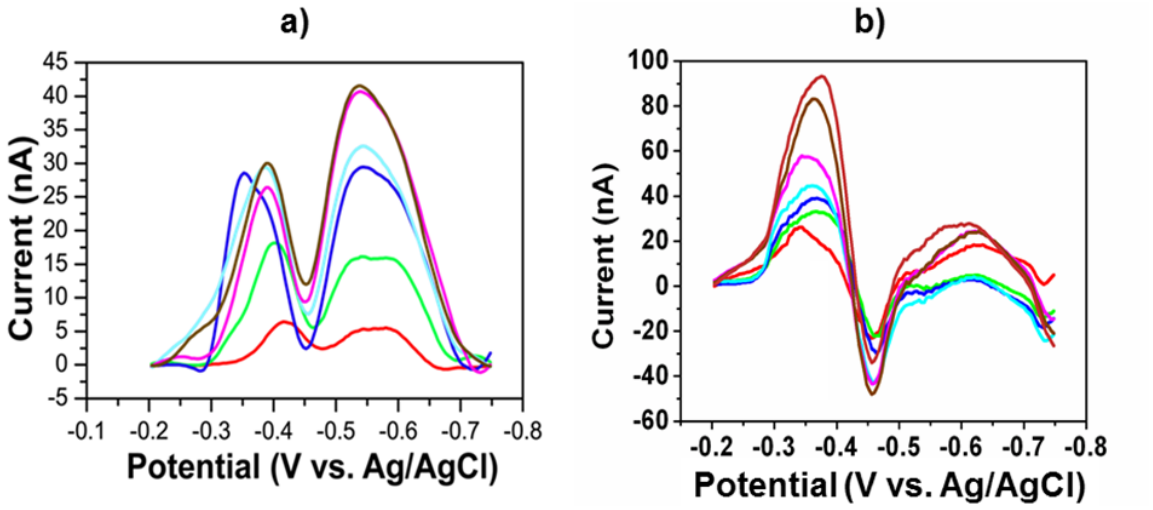

Figure 4.2: Background subtracted SWV data obtained when the a) me.273 electrode and b) wt.273 electrode was exposed to 100 μM BPDE for 15 s to 600 s.

at -0.37 V, the -0.55 V peak exhibits larger growth over the exposure time when BPDE was exposed to me.273.

Similar to data shown in Chapter 3, electrochemical responses at me.273 were dependent on BPDE concentration. **Figure 4.3a** shows background subtracted SWV responses at 600 s for me.273 exposed to increasing concentrations of BPDE. The peak currents at both -0.37 V and -0.55 V increased as a function of BPDE concentration. The magnitude of the C_{12}Viologen peak current increase at me.273 vs. wt.273 is also of interest. Under similar BPDE exposure conditions, C_{12}Viologen peak current for me.273 at -0.37 V is approximately 50% of that at wt.273, while at -0.55 V there is an approximate 3-fold increase compared to response at wt.273. These peak current fluctuations are meaningful and the importance of this will be discussed in more detail below. **Figure 4.3b** plots the peak current at -0.55 V vs. BPDE exposure time. This data shows that the BPDE-DNA reaction exhibits a time-dependent response as a function of

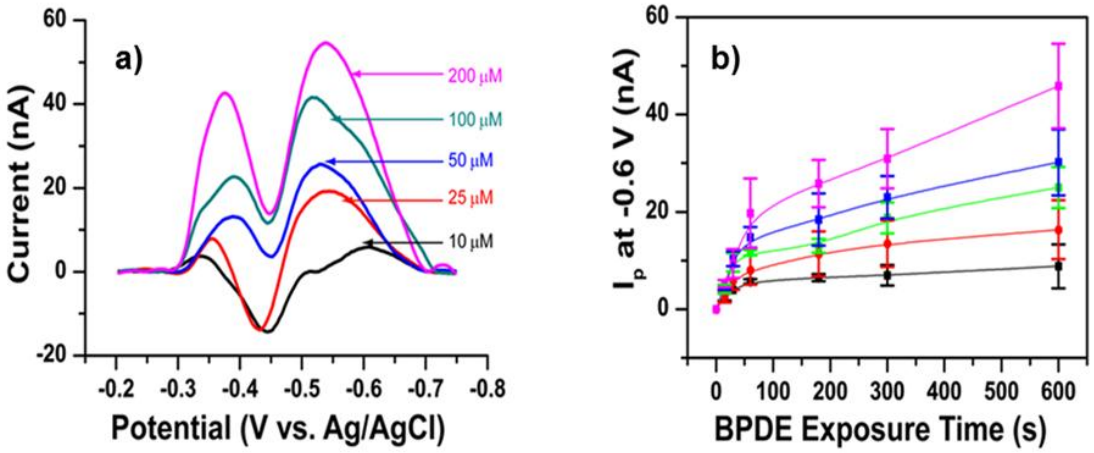

Figure 4.3: a) Background subtracted SWV plots comparing the C12Viologen reduction on a me.273 electrode exposed to varying BPDE concentrations of 10 µM to 200 µM for 600 s. b) A plot of the peak current versus the BPDE exposure time for electrodes that are exposed to different BPDE concentrations.

BPDE concentration. Compared to the response at wt.273, the reaction is slower denoted by the less steep initial slopes in the timed plot. Unlike the wt.273 sequence, the slope continues to exhibit mild increase after BPDE exposure for 300 s. This suggests that the initial reaction is similar to that at wt.273, but a secondary process is likely occurring over longer exposure times.

Controls

Similar control experiments were performed to show that BPDE was responsible for the SWV response seen at me.273. Controls included exposing alternate xenobiotics SO and BP to me.273. **Figure 4.4** shows background SWV plots comparing the responses obtained from each of these xenobiotics. The data shows that the peaks at -0.37 V and -0.55 V are dependent upon the

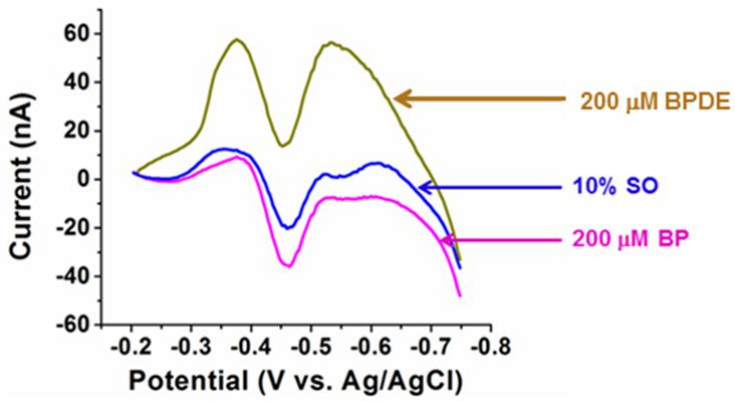

Figure 4.4: Background subtracted SWV data comparing the C12Viologen reduction when the me.wt.273 modified electrode was exposed to 200 µM BPDE (brown), 10% SO (blue) or 200 µM BP (pink).

xenobiotic used. Larger current responses are seen when BPDE was exposed to me.273 compared to muted signals observed when BP or SO were exposed to me.273. Muted signals at both -0.37 V and -0.55 V upon SO or nonmetabolized BP exposure demonstrate the sensor is sensitive to BPDE damage.

Mass Spectrometry Studies

MS studies on me.273 exposed to BPDE in solution were conducted to quantify the number of BPDE adducts on the oligomer, and provide insight into the BPDE reaction at me.273. **Figure 4.5** shows the spectrum obtained upon ESI-MS analysis. Similar to previous discussion in Chapter 3, dehybridizing ESI conditions cause the appearance of individual ssDNA m/z in the spectrum. Sodium adduction adds to the spectral complexity. The mass spectrum shows BPDE single adducts on both ss1 and ss2 with no evidence of double BPDE adduction.

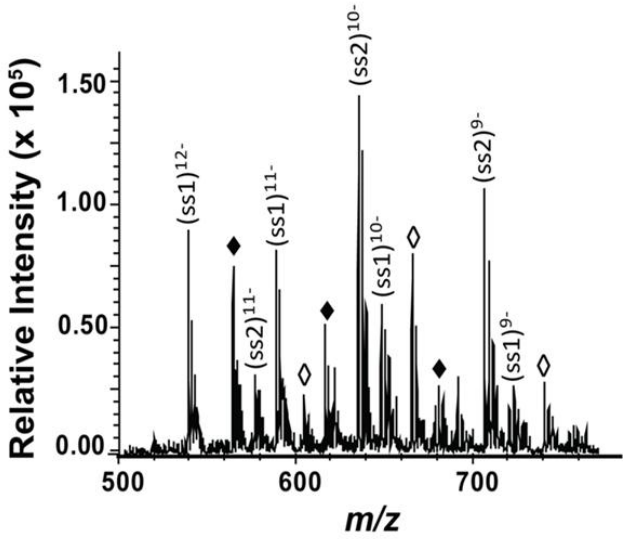

Figure 4.5: Mass spectrum showing the charge state distribution after the me.273 sequence had been exposed to BPDE.

Discussion

Electrochemical measurements showed that DNA methylation alters the resultant C_{12}Viologen voltammetry upon exposure to BPDE. Not only was the -0.37 V peak observed but

the -0.55 V peak increased much more than was seen for wt.273. The only difference between wt.273 and me.273 is the inclusion of a cytosine methyl group within the latter sequence. The me.273 electrochemical response must therefore be due to effects imparted by the cytosine methyl group that affects the resulting BPDE adduct formation and orientation.

The methyl group at the 5-C position of cytosine protrudes into the major groove of the DNA helix, shown in **Figure 4.6b**.[5-7] Cytosine methylation has a significant impact on characteristics of dsDNA.[7] Specifically, there is an increase in the hydrophobic base-stacking interaction and an increase in polarizablity which can influence the conformational state. [7-9] Studies have shown that the methyl group can facilitate and induce a conformational change when BPDE adducts guanine.[7] **Figure 4.7** once again shows the two pair of enantiomeric

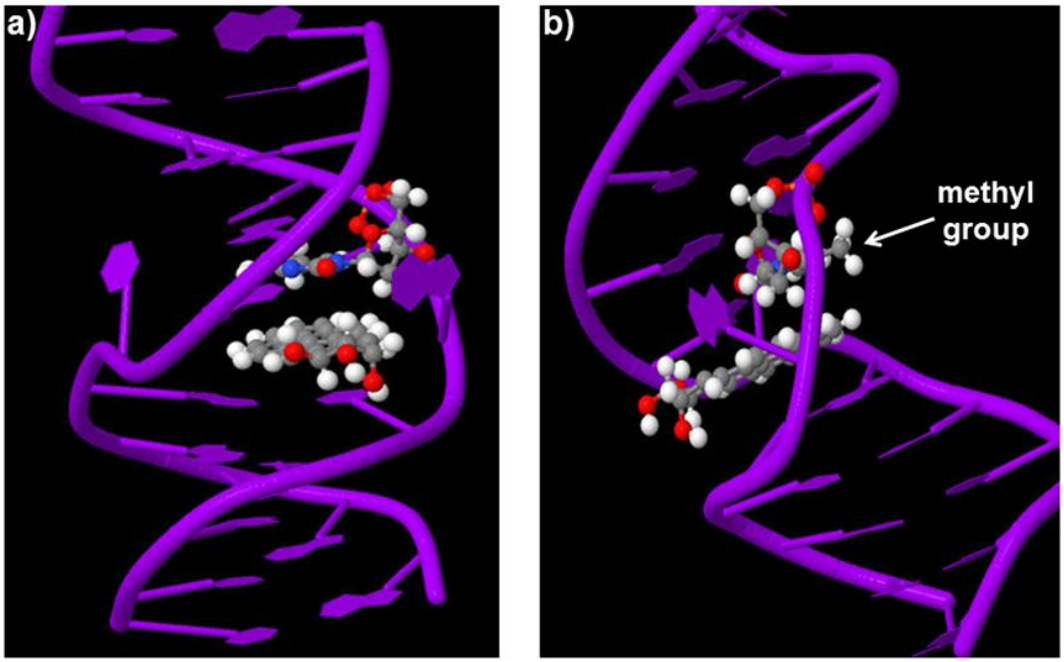

Figure 4.6: Space filled model of a methylated DNA sequence a) (-)-*trans*-*anti*-[BP]-N^2-guanine adduct intercalating causing displacement of base-pairing b) a 90º counterclockwise view to provide visual of both grooves when (-)-*trans*-*anti*-BPDE is adducted. Reprinted with permission from PDB ID: 1Y9H Zhang, N.; Lin, C.; Huang, X.; Kolbanovskiy, A.; Hingerty, B. E.; Amin, S.; Broyde, S.; Geacintov, N. E.; Patel, D. J. Methylation of Cytosine at C5 in a CpG Sequence Context Causes a Conformational Switch of a Benzo[a]pyrene diol epoxide-N2-guanine Adduct in DNA from a Minor Groove Alignment to Intercalation with Base Displacement. *J. Mol. Biol.* **2005**, *346*, 951-965. Copyright 2005 American Chemical Society.

adducts formed when (±)-*anti*-BPDE reacts at the guanine N^2 amine location in DNA. The expected percentage of the products is also shown in the figure. Compared to the previous discussion using wt.273 (Chapter 3), the product distribution is expected to remain the same, but cytosine methylation will affect the orientation of certain products shown in the figure.[7] NMR studies indicated that (+)-*trans*-BPDE and (-)-*trans*-BPDE adducts will align with different spatial orientations if the cytosine 5' to the damaged guanine. The (+)-*trans*-*anti*-[BP]-N^2-guanine will remain minor groove bound while (-)-*trans*-*anti*-[BP]-N^2-guanine transitions to a base-displacing intercalating adduct (**Figure 4.6a**). The methyl group on the cytosine 5' to the guanine essentially acts to pull the (-)-*trans*-BP adduct into the helix interior. The influence of the methyl group on the orientation of this stereochemical adduct is shown in **Figure 4.6**. The added hydrophobic interactions compensate for the loss in base pairing. The (-)-*cis*-BP adduct remains a base-displacing intercalating adduct with similar characteristics as the (-)-*trans*-BP adduct.

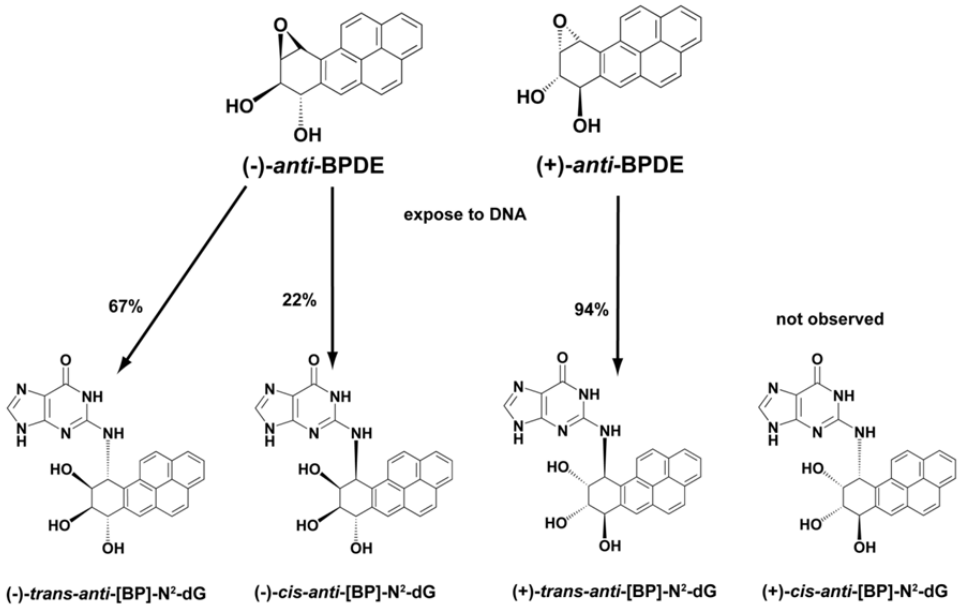

Figure 4.7: The racemic mixture of BPDE exposed to DNA gave rise to two different adducts with different configurations per enantiomer.

Me.273 was exposed to a racemic (±)-*anti*-BPDE solution. DNA was therefore exposed to (+)-*trans*-BPDE and (-)-*trans*-BPDE in a 50/50 ratio. The expected products resulting from DNA exposure to this solution are roughly 50% adducts located in the minor groove (from (+)-*trans*-BPDE) and 50% base-displacing intercalating adducts (from (-)-*trans*-BPDE or (-)-*cis*-BPDE). This even split is different than the expected product distribution using wt.273 where the majority of expected adducts were minor groove bound. These percentages explain the electrochemical differences observed in the me.273 vs. wt.273.

The me.273 SWV plot showed the peak currents at -0.37 V and -0.55 V to be roughly equal in magnitude. Compared to the wt.273 response, current decreases at -0.37 V can be explained by only (+)-*trans*-*anti*-BPDE binding in the minor groove in the me.273 case. Formerly, both (+)-*trans*-*anti*-BPDE and (-)-*trans*-*anti*-BPDE were expected to be bound in the minor groove on wt.273.[10] Increase in the electrochemical signal at -0.55 V is consistent with the changing orientation of (-)-*trans*-*anti*-BPDE from minor groove bound to an intercalating conformation, in addition to (-)-*cis*-*anti*-BPDE remaining in a similar intercalating orientation.[7] Positive shifts in C_{12}Viologen reduction current compared to the formal potential (~0.45 V) were previously assigned to viologen dimerization within the DNA minor groove. The methyl group acts to force the intercalation of BP-moieties accompanied by base displacement.[4, 7] The displaced bases are the guanine on which the BPDE binds as well as the opposite cytosine on the complementary ssDNA. The cytosine is displaced into the major groove, while the displaced guanine bases are positioned within the minor groove, which may facilitate some sort of π-interactions among C_{12}Viologen. The viologen interaction within the minor groove stabilizes oxidized C_{12}Viologen (V^{2+}) as the reduction peak is shifted negative. Stabilization could originate from electrostatic or hydrogen bonding interactions within the minor groove. The base

displacement likely causes C_{12}Viologen aggregation and dimerization resulting in the large current increase at approximately -0.55 V upon reduction under the experimental viologen solution concentration conditions used here. Overall, the single cytosine methyl group caused a conformational change in the BPDE adduct and changes in the me.273 electrochemical signal compared to wt.273.

Electrochemical and mass spectrometry data provided solid evidence that cytosine methylation influences not only the site-specific reaction but also the stereospecific binding of BPDE to DNA. When BPDE reacts at DNA, the resulting adduct orients differently within the DNA helix based on varying stereochemical parameters. The data suggests that the electrochemical sensor can effectively detect and provide sensitive voltammetric responses corresponding to the different stereochemical conformations involved in BPDE adduction at hotspot DNA sequences.

References

(1) Tornaletti, S.; Pfeifer, G. P. Complete and tissue-independent methylation of CpG sites in the p53 gene: implications for mutations in human cancers. *Oncogene* **1995**, *10*, 1493.

(2) Denissenko, M. F.; Pao, A.; Tang, M.; Pfeifer, G. P. Preferential Formation of Benzo[*a*]pyrene Adducts at Lung Cancer Mutational Hotspots in P53. *Science* **1996**, *274*, 430-432.

(3) Chen, J. X.; Zheng, Y.; West, M.; Tang, M. Carcinogens Preferentially Bind at Methylated CpG in the p53 Mutational Hot Spots. *Cancer Research* **1998**, *58*, 2070-2075.

(4) Weisenberger, D. J.; Romano, L. J. Cytosine Methylation in a CpG Sequence Leads to Enhanced Reactivity with Benzo[*a*]pyrene Diol Epoxide That Correlates with a Conformational Change. *Journal of Biological Chemistry* **1999**, *274*, 23948-23955.

(5) Matter, B.; Wang, G.; Jones, R.; Tretyakova, N. Formation of Diastereomeric Benzo[*a*]pyrene Diol Epoxide-Guanine Adducts in p53 Gene-Derived DNA Sequences. *Chemical Research in Toxicology* **2004**, *17*, 731-741.

(6) Nagalingam, A.; Seo, K.; Loechler, E. L. Mutagenesis studies of the major benzo[*a*]pyrene N2-dG adduct in a 5′-TG versus a 5′-UG sequence: removal of the methyl group causes a modest decrease in the [G→T/G→A] mutational ratio. *Mutagenesis* **March 2005**, *20*, 105-110.

(7) Zhang, N.; Lin, C.; Huang, X.; Kolbanovskiy, A.; Hingerty, B. E.; Amin, S.; Broyde, S.; Geacintov, N. E.; Patel, D. J. Methylation of Cytosine at C5 in a CpG Sequence Context Causes a Conformational Switch of a Benzo[*a*]pyrene diol epoxide-N2-guanine Adduct in DNA from a Minor Groove Alignment to Intercalation with Base Displacement. *Journal of Molecular Biology* **2005**, *346*, 951-965.

(8) Denissenko, M. F.; Chen, J. X.; Tang, M.; Pfeifer, G. P. Cytosine methylation determines hot spots of DNA damage in the human P53 gene. *Proceedings of the National Academy of Sciences* **1997**, *94*, 3893-3898.

(9) Yoon, J.; Smith, L. E.; Feng, Z.; Tang, M.; Lee, C.; Pfeifer, G. P. Methylated CpG Dinucleotides Are the Preferential Targets for G-to-T Transversion Mutations Induced by Benzo[*a*]pyrene Diol Epoxide in Mammalian Cells. *Cancer Research* **2001**, *61*, 7110-7117.

(10) Geacintov, N.; Cosman, M.; Hingerty, B.; Amin, S.; Broyde, S.; Patel, D. NMR solution structures of stereoisometric covalent polycyclic aromatic carcinogen-DNA adduct: principles, patterns, and diversity. *Chemical Research in Toxicology* **1997**, *10*, 111-146.

CHAPTER 5: ELECTROCHEMICAL DETECTION OF DNA DAMAGE AT TP53 OLIGOMERS FROM IN SITU GENERATED REACTIVE BENZO[*A*]PYRENE SPECIES

Results

Electrochemical Detection

In addition to wt. 273, gold electrodes were modified with 21-mer oligomeric DNA sequence spanning codons 243-249 of the TP53 gene, named wt.248.245. Specifically, this sequence contains the reaction hotspot guanines within codons 245 and 248. These guanines have been shown to be high mutation frequency sites in lung cancer.[1] Wt.248.245 modified electrodes were exposed to BPDE precursor BP in a reactive buffer solution in order to ascertain the consequences of BP bioactivation in the hotspot DNA damage process.

Typically, bioactivation involves enzymatic conversion of a substrate into a reactive product. In the case of BP, the first enzymatic process is epoxidation by heme enzymes; typically cyt P450s. In initial studies, a heme enzyme mimic was used to study this process. Myoglobin (Mb) was utilized as it has been shown to exhibit oxidase properties under certain conditions.[2] Mb can be activated using small amounts of H_2O_2 to activate the heme center to a reactive intermediate.[2] This mechanism is termed the peroxide shunt.[2] Similar experiments as described in Chapters 3 and 4 were performed using BP at a desired concentration along with nM concentrations of H_2O_2 and Mb mixed in a reaction cocktail buffer and exposed to electrodes modified with either wt.248.245 or wt.273. Electrochemical measurements were performed after the damage reaction. **Figure 5.1** shows the background subtracted SWV responses for wt.273 exposed to these conditions. Data in **Figure 5.1** shows some very interesting metabolism/reaction related phenomena. First, exposure to only H_2O_2 produces very little current increase suggesting this component alone contributes very little toward DNA damage. When all three components (Mb, BP and H_2O_2) were mixed and exposed to wt.273, a significant current

increase occurred at approximately -0.50 V. Current increase at this potential is consistent with the generation of a nucleobase-displacement intercalating BP adduct, presumably generated by Mb metabolism. Very little current increase at -0.37 V suggests that the BP adduct is not primarily bound within the minor groove.

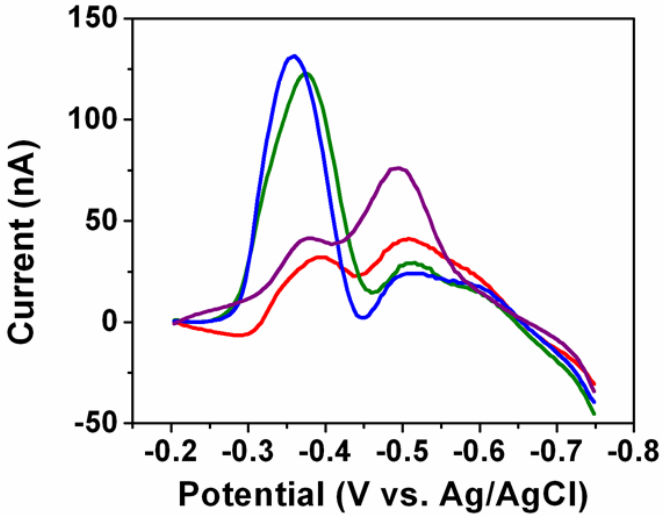

Figure 5.1: Background subtracted SWV illustrating voltammetric responses for wt.273 being exposed to 250 μM H_2O_2 only (red), 3 mg/mL Mb + 100 μM BP + 250 μM H_2O_2 (purple), 100 μM BP + 250 μM H_2O_2 (green) and 100 μM BP + 500 μM H_2O_2 (blue).

Another interesting aspect in the **Figure 5.1** plot is the large peak current generation at -0.37 V seen after exposure to the combination of only H_2O_2 and BP. Current increase at -0.37 V is similar to the BPDE reactions at wt.273, which were assigned to minor groove bound BP adducts. Because of the magnitude of the peak current in relation to the other current increases, additional aspects of this reaction were explored. **Figure 5.2** shows a background subtracted SWV response comparison between wt.248.245 and wt.273 exposed to 5 μM BP and 250 μM H_2O_2 from 15-600 s. **Figure 5.2** shows that the C_{12}Viologen electrochemical response for the single codon (wt.273, **Figure 5.2a**) and double codon (wt.248.245, **Figure5.2b**) both showed significant peak growth at -0.37 V when exposed to BP and H_2O_2. Peak growth at this location is consistent with minor groove located BP adducts as described previously. The main

difference between the plots is the large change in -0.37 V peak current at wt.248.245 vs. wt.273. The difference between the two sequences is the inclusion of a second hotspot CpG dinucleotide sequence in wt.248.245. The second reaction site in wt.248.245 presumably enhances the damage reaction rate resulting in increased DNA damage over the exposure period.

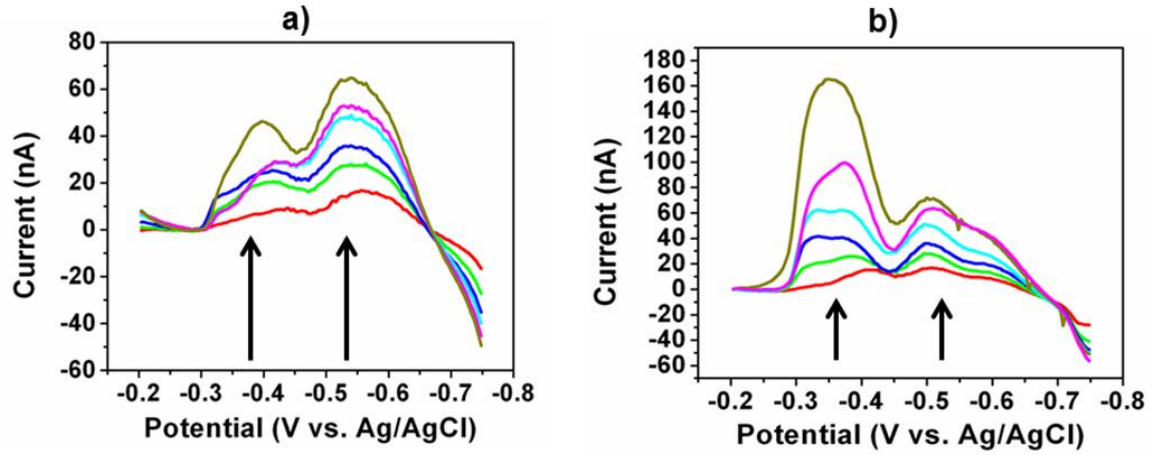

Figure 5.2: Background subtracted SWV data for when a) wt.273 and b) wt.248.245 were exposed to 5 μM BP and 250 μM H_2O_2 for 15-600 s.

The potential at approximately -0.50 V also shows significant growth over exposure time for both modified electrodes, yet the peak currents result in approximately equal intensities. The reasons for the equal peak current intensity on the two different DNA sequence is not completely understood, but the growth in peak current at this location is consistent with base-displacing intercalating BP adducts.

Figure 5.3 shows that the -0.37 V peak height was dependent upon the concentration of BP and H_2O_2 exposure as well as the DNA sequence used. The figure shows the average -0.37 V peak height for 3 min BP-H_2O_2 exposure (n = 3) at wt.273 or wt.248.245. Based on the initial slopes of the data, the damage reaction occurs slightly faster at wt.248.245. In addition, after an initial fast reaction at low BP concentrations for both oligomers, the peak height levels off for wt.273 while it continues to grow at wt.248.245. Slower peak growth at higher BP

concentrations on wt.248.245 indicates that there is a slower secondary reaction after the initial DNA reaction sites have been saturated. This is indicative of a surface with both easily accessible reaction sites in conjunction with secondary sites, which is consistent with DNA exhibiting two reactive guanine sites. Higher signals obtained when BP and H_2O_2 were exposed to wt.248.245 demonstrate the importance of the two hotspot codon sites in the sequence. Two hotspot sites provide additional positions for xenobiotics to preferentially adduct, which dramatically alters DNA morphology and the resulting voltammetry.

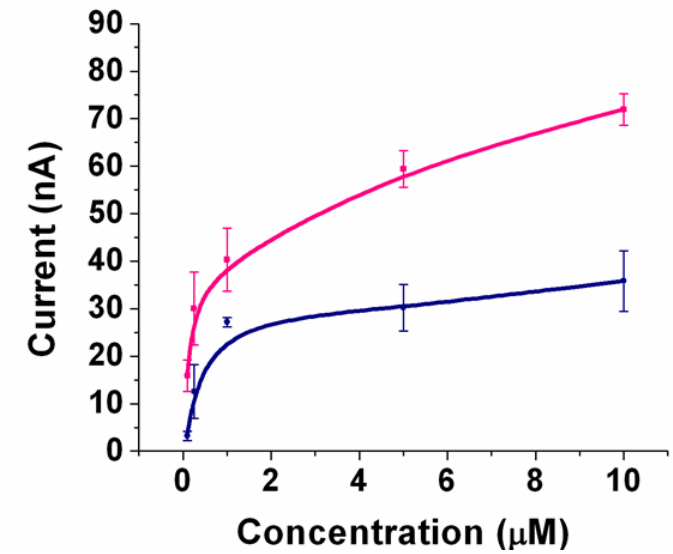

Figure 5.3: Plot of concentration versus peak current when electrodes are exposed to increasing BP concentrations and 250 μM H_2O_2 at 180 s. Wt.248.245 (pink) and wt.273 (blue) exposed to reaction conditions.

Controls

Control experiments were performed to show that the combination of BP and H_2O_2 were responsible for the SWV response at -0.37 V. Controls included exposing wt.248.245 to H_2O_2 only and a reaction between THF and H_2O_2. THF was used to solubilize BP; therefore, it was a concern that this solvent may be reacting at DNA in conjunction with H_2O_2 to produce the large positively shifted peak in the bioactivation solution. **Figure 5.4** shows background subtracted SWV responses comparing these controls. The data show that neither THF nor H_2O_2 conditions

strongly influence the current at -0.37 V or -0.53 V. Overall, these controls provide evidence that the peaks at -0.37 V and -0.53 V are due to C_{12}Viologen interacting at DNA damaged sites from the combination of BP and H_2O_2.

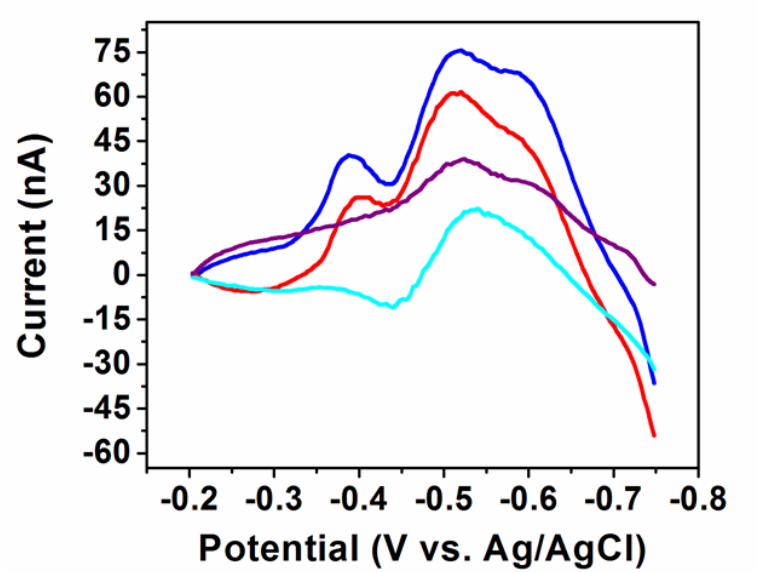

Figure 5.4: Background subtracted SWV plot when wt.248.245 electrode was exposed to 10 μM THF and 250 μM H_2O_2 (cyan), 250 μM H_2O_2 only (purple), 250 nM BP and 250 μM H_2O_2 (red), and 500 nM BP and 250 μM H_2O_2 (blue) for 180 s exposure time.

Because the reaction of hydrogen peroxide and alkenes is known to be extremely sluggish in solution without the addition of a catalyst, it was hypothesized that a second reaction was occurring in solution involving the production of a hydroxyl radical.[3] Generated hydroxyl radicals could then activate BP facilitating reaction at guanine. In order to determine if this was the case, a control experiment was performed using butylated hydroxyanisole (BHA), a hydroxyl radical scavenger, in conjunction with the BP-H_2O_2 reaction. BHA is known to react with free radicals; therefore, if these were present in our solution, the reaction rate would be slowed upon its inclusion. **Figure 5.5** shows background subtracted SWV responses at 600 s for wt.248.245 exposed to 200 μM BP, 250 μM H_2O_2 and 50 μM BHA. These data show that the peak current intensities are dramatically muted upon the inclusion of BHA. The peak at -0.37 V essentially

disappears upon its inclusion. The disappearance of this peak suggests that the BP adducts do not form in significant amounts when BHA is present in solution. Since BHA reacts with radicals in solution, these data suggest that the large peak currents from BP-H_2O_2 exposure were due to BP

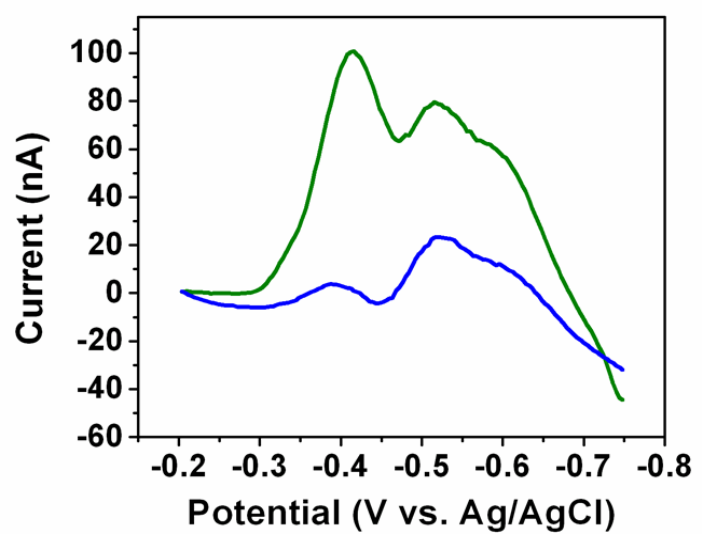

Figure 5.5: Background subtracted SWV plot when wt.248.245 electrode was exposed to a) 200 μM BP, 250 μM H_2O_2 and 50 μM $C_{11}H_{16}O_2$ (butylated hydroxyanisole, BHA) (blue) b) 100 μM BP and 250 μM H_2O_2 (green) for 600 s.

activation by hydroxyl radicals followed by activated BP adducting at guanine hotspot sites within the DNA.

BHA elucidated the presence of hydroxyl radicals in the reaction solution, but the source of radical generation was unclear. To determine this information, an additional control using ethylenediaminetetraacetic acid (EDTA) was performed to determine the origin of the hydroxyl radical. EDTA is a chelating agent responsible for sequestering certain metal ions.[4, 5] Previous studies using biological systems showed that hydroxyl radicals were produced when metal complexes reacted with H_2O_2 in a Fenton-type reaction.[4, 5] Metal impurities present during damage experiments would explain the generation of hydroxyl radicals in our system. **Figure 5.6** shows a background subtracted SWV response at 600 s for wt.248.245 exposed to 100 μM BP, 250 μM H_2O_2 and 50 μM EDTA. The muted signal response at -0.37 V demonstrates that the BP

activation is essentially stopped in the presence of EDTA. This is consistent with the sequestering of trace redox metals by EDTA, eliminating the hydroxyl radical generating catalyst.

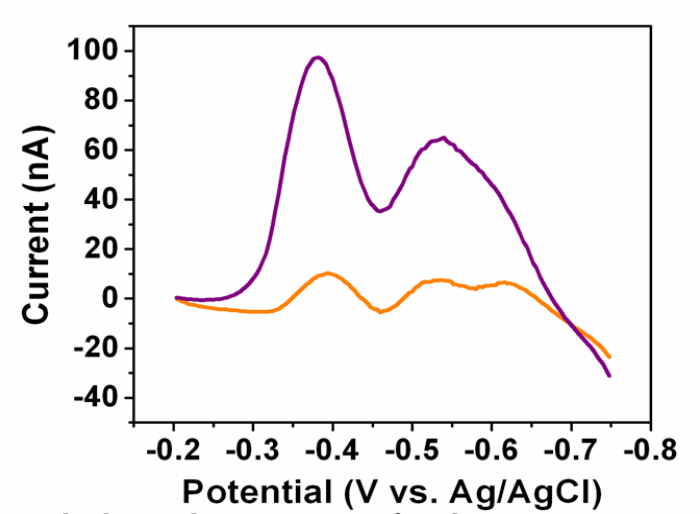

Figure 5.6: Background subtracted SWV response for when wt.248.245 was exposed to a) 100 μM BP, 250 μM H_2O_2 and 50 μM EDTA (orange) and b) 100 μM BP and 250 μM H_2O_2 (purple) for 600 s.

Discussion

Electrochemical measurements performed after Au electrodes were exposed to different combinations of Mb, BP and H_2O_2 showed changes in the resultant C_{12}Viologen voltammetry. Wt.248.245 exposed to all three components exhibited a large increase at approximately -0.50 V. Increase at this population suggests that BP is metabolized by Mb presumably resulting in intercalating-type DNA adducts. The large peak current observed at -0.37 V seen after exposure to only BP and H_2O_2 was unexpected. This current increase is consistent with minor groove bound BP adducts. Experimental results showed that the -0.37 V peak current was dependent upon the number of hotspots present in the sequence. Wt.248.245 has two hotspot codons BP reacts both faster and in higher amounts at this sequence.

The large -0.37 V current response seen in the BP-H_2O_2 studies indicates that the combination of these substrates results in an active BP form, despite the lack of enzyme in

solution. A second underlying reaction must be occurring to explain the large peak current increase at -0.37 V. It was hypothesized that the reaction must involve the production of a hydroxyl radical. The -0.37 V peak decreased when BHA was present in the reaction solution, suggesting that BP is not activated in these solutions presumably because BHA acts as a radical scavenger. Signals also decreased using EDTA, suggesting that metal ions reacted with hydrogen peroxide to produce reactive radicals. These data are all consistent with hydroxyl radical generation by a Fenton reaction. The electrochemical data suggests that the generated hydroxyl radical activates BP leading to adduct formation on guanine. A proposed mechanism is shown below.[6-8]

(1) $Fe^{2+} + H_2O_2 \rightarrow Fe^{3+} + OH^- + \bullet OH$

(2) $Fe^{3+} + H_2O_2 \rightarrow Fe^{2+} + OOH\bullet + H^+$

(3) $\bullet OH + BP \rightarrow BP^*$

(4) $BP^* + DNA_{gua} \rightarrow DNA{-}BP_{gua}$

Studies have shown that significant amounts of •OH can be produced even in situations where iron is not in large excess.[4, 7] There was no direct addition of iron in the system studied here suggesting that the Fe must originate from impurities in buffer components. The buffer components all have trace Fe impurities. The concentrations of these impurities in our bulk NaCl and Tris were reported to be 2.0 ppm and 5.0 ppm respectively based on the distributor information. Each of these components is 10 mM in the E-buffer, which equates to roughly 0.13 μM of Fe in solution. In addition, impurities from our bulk phosphate buffer were reported to have unidentified heavy metal impurities not exceeding 5 ppm, which equates to an absolute maximum of 0.80 μM of Fe in the damage solution. This concentration is most certainly high enough to produce a Fenton reaction in our damage buffer.

A great deal of interest in free radical DNA damage has been reported.[9, 10] Free radicals are of high biological importance because they influence many biological systems. Free radicals can react directly at DNA or they can react with other molecules influencing their toxicity. For instance, free radicals produced in tobacco smoke elevate the toxicity of the chemicals within the smoke. Inclusion of a free radical scavenger in a cigarette filter decreased the toxicity of cigarette smoke to cells upon exposure.[11] In addition, studies showed that non-enzymatically activated BP formed adducts on calf thymus DNA in solution.[9] It was hypothesized that BP was activated by both a Fenton-type reaction and also autoxidation processes.[9] These findings are consistent with the electrochemical results presented here.

Overall, our results are consistent with Fenton chemistry occurring in the DNA damage buffer leading to H_2O_2 activation to hydroxyl radicals. Hydroxyl radicals appear to activate BP to a reactive species producing DNA adducts at wt.248.245 and wt.273 modified surfaces. The reaction occurred faster and at elevated levels using wt.248.245 presumably due to the presence of two reactive codons in the DNA sequence. Despite the lack of enzymatic bioactivation, these findings are biologically relevant as it has been shown that BP-DNA adducts can be formed by exposing cellular DNA to xenobiotics in the presence of reactive oxygen species (ROS). Using our previous BPDE results as a guide, these data suggest that ROS activation of BP results in minor groove located DNA adducts as large peak current growth at -0.37 V was detected using SWV. (+)-*trans*-BPDE is known to be mutagenic, while (-)-*trans*-BPDE is not.[12] The difference in mutagenicity is influenced by DNA morphology differences based on the adduct orientation within DNA, as the (+) enantiomer is located in the minor groove, and the (-) enantiomer intercalates mainly due to cytosine methylation (see Chapter 4). Since our results suggest primarily minor groove located adducts, this may help to explain the toxicity induced through the

exposure of cells to the synergistic mixture of ROS and xenobiotics like BP. Future studies will continue to explore this synergistic reaction.

References

(1) Smith, L. E.; Denissenko, M. F.; Bennett, W. P.; Li, H.; Amin, S.; Tang, M.; Pfeifer, G. P. Targeting of Lung Cancer Mutational Hotspots by Polycyclic Aromatic Hydrocarbons. *Journal of the National Cancer Institute* **2000**, *92*, 803-811.

(2) Rusling, J. F.; Hvastkovs, E. G.; Hull, D. O.; Schenkman, J. B. Biochemical applications of ultrathin films of enzymes, polyions and DNA. *Chemical Communications* **2008**, 141-154.

(3) Yao, H.; Richardson, D. E. Epoxidation of Alkenes with Bicarbonate-Activated Hydrogen Peroxide. *Journal of the American Chemical Society* **2000**, *122*, 3220-3221.

(4) Prigodich, R. V.; Martin, C. T. Reaction of single-stranded DNA with hydroxyl radical generated by iron(II)-ethylenediaminetetraacetic acid. *Biochemistry* **1990**, *29*, 8017-8019.

(5) Gutteridge, J. M. C. Ferrous salt-promoted damage to deoxyribose and benzoate. The increased effectiveness of hydroxyl radical scavengers in the presence of EDTA. *Biochemical Journal* **1987**, *243*, 709-714.

(6) Prousek, J. Fenton chemistry in biology and medicine. *Pure and Applid Chemistry* **2007**, *79*, 2325-2338.

(7) Termini, J. Hydroperoxide-induced DNA damage and mutations. *Mutation Research/Fundamental and Molecular Mechanisms of Mutagenesis* **2000**, *450*, 107-124.

(8) Lloyd, R. V.; Hanna, P. M.; Mason, R. P. The Origin of the Hydroxyl Radical Oxygen in the Fenton Reaction. *Free Radical Biology and Medicine* **1997**, *22*, 885-888.

(9) Bryla, P.; Weyand, E. H. Role of activated oxygen species in benzo[*a*]pyrene: DNA adduct formation in vitro. *Free Radical Biology and Medicine* **1991**, *11*, 17-24.

(10) Marnett, L. J.; Reed G.A. Peroxidatic oxidation of benzo(*a*)pyrene and prostaglandin biosynthesis. *Biochemistry* **1979**, *18*, 2923.

(11) Alexandrov, K.; Rojas, M.; Rolando, C. DNA Damage by Benzo(*a*)pyrene in Human Cells Is Increased by Cigarette Smoke and Decreased by a Filter Containing Rosemary Extract, Which Lowers Free Radicals. *Cancer Research* **2006**, *66*, 11938-11945.

(12) Geacintov, N.; Cosman, M.; Hingerty, B.; Amin, S.; Broyde, S.; Patel, D. NMR solution structures of stereoisometric covalent polycyclic aromatic carcinogen-DNA adduct: principles, patterns, and diversity. *Chemical Research in Toxicology* **1997**, *10*, 111-146.

CHAPTER 6: CONCLUSIONS

The intent of these investigations was to determine if the electrochemical platform could detect DNA damage from the carcinogen (BPDE) or procarinogen (BP) at site-specific TP53 locations.

BPDE exposure to DNA that was immobilized on an electrode caused helix morphology changes, resulting in an altered C_{12}Viologen SWV voltammetry signal. BPDE-damaged DNA oligomers consisting of a sequence surrounding hotspot codon 273 of the TP53 gene (wt.273) exhibited a current increase at -0.37 V upon reduction of C_{12}Viologen. Current increase at this location is consistent with viologen dimerization due to C_{12}Viologen aggregation at damaged DNA sites.[1] The large increase in electrochemical signal at this location was explained by the BPDE adduct stereochemistry. Wt.273 was exposed to a racemic (±)-*anti*-BPDE solution. (-)-*trans*-BPDE and (+)-*trans*-BPDE both primarily generate minor groove located adducts when bound to guanines in DNA (**Figure 3.16**).[2, 3] These types of adducts protrude slightly from the DNA helix, producing a large hydrophobic site where C_{12}Viologen can aggregate, and dimerize upon electrochemical reduction. The positive shifted potential is consistent with a less stable bound oxidized C_{12}Viologen (V^{2+}) form that does not experience the same stabilizing interaction as electrostatic or minor groove bound populations.[1]

Control experiments using SO and nonmetabolized BP showed very little current change at -0.37 V, demonstrating the sensor was sensitive to BPDE damage. Muted signals observed in these control experiments are consistent with the different orientations that these xenobiotics adopt when bound on or within DNA. An additional control where the codon 273 guanine was swapped with cytosine provided a muted -0.37 V C_{12}Viologen reduction peak. This data along with mass spectrometry and thermal melting analysis showed that BPDE preferentially adducts the codon 273 guanine in wt.273 oligomers. Overall, the hybridized sensor was able to detect not

only sequence specific DNA damage from BPDE, but the acquired voltammetric signals were due to the stereochemistry of the adduct on the helix.

As an extension to the wt.273-BPDE study, we explored how cytosine methylation, which occurs at a large number of CpG sites, affected BPDE adduct formation. Methylation of the target complementary ssDNA at the cytosine 5' to the guanine in the codon 273 sequence provided methylated dsDNA oligomers (me.273). Similar electrochemical experiments as those using wt.273 showed that BPDE damage caused altered C_{12}Viologen voltammetry. BPDE-damaged me.273 exhibited a current increase at both -0.37 V and -0.55 V. Current increase at -0.37 V was approximately 50% of that at wt.273. Conversely, at -0.55 V, an approximate 3-fold increase was seen. The different electrochemical response demonstrates the methyl group did influence the binding of BPDE to the DNA oligomer. The voltammetry is consistent with stereochemical changes that BPDE undergoes when bound to methylated oligomers. The -0.37 V peak still correlates with a minor groove bound species. (+)-*trans*-BPDE has been shown to align in the DNA minor groove in the presence of methylated oligomers because it is not influenced by the methylated cytosine.[4, 5] Negative shifts in peak potential using C_{12}Viologen have been previously assigned to minor groove bound dimers upon one-electron reduction.[4-6] Therefore, we postulated that the current increase at -0.55 V was due to a similar process. (-)-*trans*-BPDE is known to be influenced by the methylated cytosine and transitions from minor groove to an intercalated form causing displacement of the guanine-cytosine base pair on which it is bound (**Figure 4.6**).[4-6] This process might result in a minor groove aggregation site for C_{12}viologen resulting in the negative shifted current. Additionally, (-)-*cis*-BPDE produces a similar type of adduct. These two contributions to DNA damage would create a situation where 50% of the

DNA adducts are minor groove located while 50% are base displaced-intercalated. These adduct types would lead to two different C_{12}Viologen populations and two different SWV signals

Xenobiotic bioactivation can generate reactive species that may damage biomaterial. The previous two studies involved directly damaging DNA with the reactive BPDE metabolite; therefore, studies were performed to determine if enzyme systems could be incorporated into the sensor to detect sequence specific DNA damage from *in situ* generated reactive species. Implementation of the enzyme system using Mb, BP and H_2O_2 showed changes in the resultant C_{12}Viologen voltammetry. Wt.248.245 exposed to all three components exhibited significant increase at -0.50 V which is consistent with an intercalating BP-DNA adduct. Studies involving Mb will be explored further in the future. The most interesting aspect about the bioactivation studies was the large current increase at -0.37 V upon exposure with BP and H_2O_2 in the absence of Mb. This current increase at -0.37 V is similar to the BPDE reaction at wt.273.Additional experimental evidence showed that a radical was generated, most likely via H_2O_2 reduction to hydroxyl radicals by small concentrations of Fe impurities.[7, 8] The hydroxyl radical then activated BP to a reactive species resulting in DNA adducts. The large current at -0.37 V suggests that these adducts are located in the minor groove of DNA. BP is known to exhibit higher toxicity in the presence of reactive oxygen species like hydroxyl radicals, and the electrochemical results presented here provide some evidence supporting these findings.[9-11] Similar adduct locations as (+)-*trans*-BPDE suggest that these reactive species form similar types of adducts, which may explain their toxicity.

The research performed and described here lays a rich groundwork for a variety of interesting future work. Future studies will involve investigating the voltammetric response when Mb, BP, H_2O_2 are exposed to oligomers. This is important because the BP metabolism appears to

alter the adduct orientation based on the positive shifted peak current obtained in our preliminary studies using Mb. Mb studies will allow the development of a protocol to eventual employ cyt P450 enzymes to be studied. Using human enzymes will provide a more accurate toxicity prediction by facilitating comparisons with established *in vivo* toxicity data. Additionally, it will be interesting to determine the cyt P450 isoforms involved in the production of different BPDE-DNA stereochemical adducts. We envision that these types of studies will allow the determination of isoforms involved in toxic bioactivation of BPDE.

Another interesting avenue to explore is the ROS activation of BP presumably resulting in minor groove bound adducts. To our knowledge, very little has been explored in this area. While it is known that BP will be activated by ROS in solution, no studies have elucidated the resulting adduct stereochemistry.[7, 9, 10] In this light, our results are potentially novel. Future experiments will focus on determining the identification of the reactive BP species using mass spectrometry, which will hopefully shed light on its binding to DNA.

Overall, these experiments showed that BPDE exposure to hotspot DNA oligomers produced SWV signals that are based not only on DNA sequence effects, but likely due to different stereochemical orientations of the adducts. This is a very exciting discovery as BPDE adduct toxicity is ultimately determined by the resulting orientation of the adduct on the helix. A sensor that could provide this type of information would represent a novel contribution to toxicity screening and eventually find potential environmental screening or industrial applications.

References

(1) Tang, X.; Schneider, T. W.; Walker, J. W.; Buttry, D. A. Dimerized-Complexes in Self-Assembled Monolayers Containing Viologens: An Origin of Unusual Wave Shapes in the Voltammetry of Monolayers. *Langmuir* **1996**, *12*, 5921-5933.

(2) Geacintov, N.; Cosman, M.; Hingerty, B.; Amin, S.; Broyde, S.; Patel, D. NMR solution structures of stereoisomeric covalent polycyclic aromatic carcinogen-DNA adduct: principles, patterns, and diversity. *Chemical Research in Toxicology* **1997**, *10*, 111-146.

(3) Xie, X.; Geacintov, N. E.; Broyde, S. Stereochemical Origin of Opposite Orientations in DNA Adducts Derived from Enantiomeric anti-Benzo[*a*]pyrene Diol Epoxides with Different Tumorigenic Potentials. *Biochemistry* **1999**, *38*, 2956-2968.

(4) Zhang, N.; Lin, C.; Huang, X.; Kolbanovskiy, A.; Hingerty, B. E.; Amin, S.; Broyde, S.; Geacintov, N. E.; Patel, D. J. Methylation of Cytosine at C5 in a CpG Sequence Context Causes a Conformational Switch of a Benzo[*a*]pyrene diol epoxide-N2-guanine Adduct in DNA from a Minor Groove Alignment to Intercalation with Base Displacement. *Journal of Molecular Biology* **2005**, *346*, 951-965.

(5) Weisenberger, D. J.; Romano, L. J. Cytosine Methylation in a CpG Sequence Leads to Enhanced Reactivity with Benzo[*a*]pyrene Diol Epoxide That Correlates with a Conformational Change. *Journal of Biological Chemistry* **1999**, *274*, 23948-23955.

(6) Glick, J.; Xiong, W.; Lin, Y.; Noronha, A. M.; Wilds, C. J.; Vouros, P. The influence of cytosine methylation on the chemoselectivity of benzo[*a*]pyrene diol epoxide-oligonucleotide adducts determined using nanoLC/MS/MS. *Journal of Mass Spectrometry* **2009**, *44*, 1241-1248.

(7) Lloyd, R. V.; Hanna, P. M.; Mason, R. P. The Origin of the Hydroxyl Radical Oxygen in the Fenton Reaction. *Free Radical Biology and Medicine* **1997**, *22*, 885-888.

(8) Prousek, J. Fenton chemistry in biology and medicine. *Pure and Applied Chemistry* **2007**, *79*, 2325-2338.

(9) Bryla, P.; Weyand, E. H. Role of activated oxygen species in benzo[a]pyrene: DNA adduct formation in vitro. *Free Radical Biology and Medicine* **1991**, *11*, 17-24.

(10) Alexandrov, K.; Rojas, M.; Rolando, C. DNA Damage by Benzo(*a*)pyrene in Human Cells Is Increased by Cigarette Smoke and Decreased by a Filter Containing Rosemary Extract, Which Lowers Free Radicals. *Cancer Research* **2006**, *66*, 11938-11945.

(11) Jackson, J. H.; Schraufstatter, I. U.; Hyslop, P. A.; Vosbeck, K.; Sauerheber, R.; Weitzman, S. A.; Cochrane, C. G. Role of oxidants in DNA damage. Hydroxyl radical mediates the synergistic DNA damaging effects of asbestos and cigarette smoke. *The Journal of Clinical Investigation* **1987**, *80*, 1090-1095.